EUROPEAN ORGANISATION FOR NUCLEAR RESEARCH

CERN-PPE/92-116
7th July 1992

Inclusive Neutral Vector Meson Production in Hadronic Z^0 Decays

The OPAL Collaboration

Abstract

Results are reported of a study of neutral vector meson production in multihadronic Z^0 decays in the OPAL experiment at LEP. Pions and kaons have been identified by specific ionisation energy loss and $K^{\pm}\pi^{\mp}$ and K^+K^- mass spectra have been fitted, in bins of the scaled momentum variable x_p, to combinations of resonance signals and non-resonant backgrounds. Rates are given for $K^*(892)^0$ and $\phi(1020)$, and production cross sections are compared to the predictions of Monte Carlo models. Overall multiplicities have been determined as $0.76 \pm 0.07 \pm 0.06$ $K^*(892)^0$ and $0.086 \pm 0.015 \pm 0.010$ $\phi(1020)$ per hadronic Z^0 decay (the quoted errors are respectively statistical and systematic). Momentum dependent distortions of the $\pi\pi$ mass spectra, possibly associated indirectly with Bose-Einstein effects, have prevented reliable measurement of the $\rho(770)^0$ cross section in this study.

(Submitted to Zeitschrift für Physik C)

The OPAL Collaboration

P.D. Acton[25], G. Alexander[23], J. Allison[16], P.P. Allport[5], K.J. Anderson[9], S. Arcelli[2], A. Astbury[28], D. Axen[29], G. Azuelos[18,a], G.A. Bahan[16], J.T.M. Baines[16], A.H. Ball[17], J. Banks[16], R.J. Barlow[16], S. Barnett[16], J.R. Batley[5], G. Beaudoin[18], A. Beck[23], J. Becker[10], T. Behnke[27], K.W. Bell[20], G. Bella[23], P. Berlich[10], S. Bethke[11], O. Biebel[3], U. Binder[10], I.J. Bloodworth[1], P. Bock[11], B. Boden[3], H.M. Bosch[11], S. Bougerolle[29], H. Breuker[8], R.M. Brown[20], A. Buijs[8], H.J. Burckhart[8], P. Capiluppi[2], R.K. Carnegie[6], A.A. Carter[13], J.R. Carter[5], C.Y. Chang[17], D.G. Charlton[8], P.E.L. Clarke[25], I. Cohen[23], J.C. Clayton1, W.J. Collins[5], J.E. Conboy[15], M. Cooper[22], M. Coupland[14], M. Cuffiani[2], S. Dado[22], G.M. Dallavalle[2], S. De Jong[8], L.A. del Pozo[5], H. Deng[17], A. Dieckmann[11], M. Dittmar[4], M.S. Dixit[7], E. do Couto e Silva[12], J.E. Duboscq[8], E. Duchovni[26], G. Duckeck[11], I.P. Duerdoth[16], D.J.P. Dumas[6], P.A. Elcombe[5], P.G. Estabrooks[6], E. Etzion[23], H.G. Evans[9], F. Fabbri[2], M. Fincke-Keeler[28], H.M. Fischer[3], D.G. Fong[17], M. Foucher[17], A. Gaidot[21], O. Ganel[26], J.W. Gary[4], J. Gascon[18], R.F. McGowan[16], N.I. Geddes[20], C. Geich-Gimbel[3], S.W. Gensler[9], F.X. Gentit[21], G. Giacomelli[2], V. Gibson[5], W.R. Gibson[13], J.D. Gillies[20], J. Goldberg[22], M.J. Goodrick[5], W. Gorn[4], C. Grandi[2], F.C. Grant[5], J. Hagemann[27], G.G. Hanson[12], M. Hansroul[8], C.K. Hargrove[7], P.F. Harrison[13], J. Hart[8], P.M. Hattersley[1], M. Hauschild[8], C.M. Hawkes[8], E. Heflin[4], R.J. Hemingway[6], R.D. Heuer[8], J.C. Hill[5], S.J. Hillier[1], T. Hilse[10], D.A. Hinshaw[18], J.D. Hobbs[8], P.R. Hobson[25], D. Hochman[26], R.J. Homer[1], A.K. Honma[28,a], C.P. Howarth[15], R.E. Hughes-Jones[16], R. Humbert[10], P. Igo-Kemenes[11], H. Ihssen[11], D.C. Imrie[25], A.C. Janissen[6], A. Jawahery[17], P.W. Jeffreys[20], H. Jeremie[18], M. Jimack[2], M. Jobes[1], R.W.L. Jones[13], P. Jovanovic[1], C. Jui[4], D. Karlen[6], K. Kawagoe[24], T. Kawamoto[24], R.K. Keeler[28], R.G. Kellogg[17], B.W. Kennedy[15], S. Kluth[5], T. Kobayashi[24], T.P. Kokott[3], S. Komamiya[24], L. Köpke[8], J.F. Kral[8], R. Kowalewski[6], J. von Krogh[11], J. Kroll[9], M. Kuwano[24], P. Kyberd[13], G.D. Lafferty[16], F. Lamarche[18], J.G. Layter[4], P. Le Du[21], P. Leblanc[18], A.M. Lee[17], M.H. Lehto[15], D. Lellouch[26], P. Lennert[11], C. Leroy[18], J. Letts[4], S. Levegrün[3], L. Levinson[26], S.L. Lloyd[13], F.K. Loebinger[16], J.M. Lorah[17], B. Lorazo[18], M.J. Losty[7], X.C. Lou[12], J. Ludwig[10], M. Mannelli[8], S. Marcellini[2], G. Maringer[3], C. Markus[3], A.J. Martin[13], J.P. Martin[18], T. Mashimo[24], P. Mättig[3], U. Maur[3], J. McKenna[28], T.J. McMahon[1], J.R. McNutt[25], F. Meijers[8], D. Menszner[11], F.S. Merritt[9], H. Mes[7], A. Michelini[8], R.P. Middleton[20], G. Mikenberg[26], J. Mildenberger[6], D.J. Miller[15], R. Mir[12], W. Mohr[10], C. Moisan[18], A. Montanari[2], T. Mori[24], M. Morii[24], T. Mouthuy[12,b], B. Nellen[3], H.H. Nguyen[9], M. Nozaki[24], S.W. O'Neale[8,c], F.G. Oakham[7], F. Odorici[2], H.O. Ogren[12], C.J. Oram[28,a], M.J. Oreglia[9], S. Orito[24], J.P. Pansart[21], B. Panzer-Steindel[8], P. Paschievici[26], G.N. Patrick[20], N. Paz-Jaoshvili[23], P. Pfister[10], J.E. Pilcher[9], D. Pitman[28], D.E. Plane[8], P. Poffenberger[28], B. Poli[2], A. Pouladdej[6], E. Prebys[8], T.W. Pritchard[13], H. Przysiezniak[18], G. Quast[27], M.W. Redmond[9], D.L. Rees[1], G.E. Richards[16], D. Robinson[8], A. Rollnik[3], J.M. Roney[9], E. Ros[8], S. Rossberg[10], A.M. Rossi[2,d], M. Rosvick[28], P. Routenburg[6], K. Runge[10], O. Runolfsson[8], D.R. Rust[12], M. Sasaki[24], C. Sbarra[8], A.D. Schaile[10], O. Schaile[10], W. Schappert[6], P. Scharff-Hansen[8], P. Schenk[28], H. von der Schmitt[11], S. Schreiber[3], C. Schwick[27], J. Schwiening[3], W.G. Scott[20], M. Settles[12], T.G. Shears[5], B.C. Shen[4], C.H. Shepherd-Themistocleous[7], P. Sherwood[15], R. Shypit[29], A. Simon[3], P. Singh[13], G.P. Siroli[2], A. Skuja[17], A.M. Smith[8], T.J. Smith[8], G.A. Snow[17], R. Sobie[28,e], R.W. Springer[17], M. Sproston[20], K. Stephens[16], J. Steuerer[28], R. Ströhmer[11], D. Strom[30], T. Takeshita[24,f], P. Taras[18], S. Tarem[26], M. Tecchio[9], P. Teixeira-Dias[11], N. Tesch[3], N.J. Thackray[1], G. Transtromer[25], N.J. Tresilian[16], T. Tsukamoto[24], M.F. Turner[5], G. Tysarczyk-Niemeyer[11], D. Van den plas[18], R. Van Kooten[8], G.J. VanDalen[4], G. Vasseur[21], C.J. Virtue[7], A. Wagner[27], D.L. Wagner[9], C. Wahl[10], J.P. Walker[1], C.P. Ward[5], D.R. Ward[5], P.M. Watkins[1], A.T. Watson[1], N.K. Watson[8], M. Weber[11], P. Weber[6], S. Weisz[8], P.S. Wells[8], N. Wermes[11], M.A. Whalley[1], G.W. Wilson[4], J.A. Wilson[1], V-H. Winterer[10], T. Wlodek[26], S. Wotton[11], T.R. Wyatt[16], R. Yaari[26], A. Yeaman[13], G. Yekutieli[26], M. Yurko[18], W. Zeuner[8], G.T. Zorn[17].

[1]School of Physics and Space Research, University of Birmingham, Birmingham, B15 2TT, UK
[2]Dipartimento di Fisica dell' Università di Bologna and INFN, Bologna, 40126, Italy
[3]Physikalisches Institut, Universität Bonn, D-5300 Bonn 1, FRG
[4]Department of Physics, University of California, Riverside, CA 92521 USA
[5]Cavendish Laboratory, Cambridge, CB3 0HE, UK
[6]Carleton University, Dept of Physics, Colonel By Drive, Ottawa, Ontario K1S 5B6, Canada
[7]Centre for Research in Particle Physics, Carleton University, Ottawa, Ontario K1S 5B6, Canada
[8]CERN, European Organisation for Particle Physics, 1211 Geneva 23, Switzerland
[9]Enrico Fermi Institute and Department of Physics, University of Chicago, Chicago Illinois 60637, USA
[10]Fakultät für Physik, Albert Ludwigs Universität, D-7800 Freiburg, FRG
[11]Physikalisches Institut, Universität Heidelberg, Heidelberg, FRG
[12]Indiana University, Dept of Physics, Swain Hall West 117, Bloomington, Indiana 47405, USA
[13]Queen Mary and Westfield College, University of London, London, E1 4NS, UK
[14]Birkbeck College, London, WC1E 7HV, UK
[15]University College London, London, WC1E 6BT, UK
[16]Department of Physics, Schuster Laboratory, The University, Manchester, M13 9PL, UK
[17]Department of Physics and Astronomy, University of Maryland, College Park, Maryland 20742, USA
[18]Laboratoire de Physique Nucléaire, Université de Montréal, Montréal, Quebec, H3C 3J7, Canada
[20]Rutherford Appleton Laboratory, Chilton, Didcot, Oxfordshire, OX11 0QX, UK
[21]DPhPE, CEN Saclay, F-91191 Gif-sur-Yvette, France
[22]Department of Physics, Technion-Israel Institute of Technology, Haifa 32000, Israel
[23]Department of Physics and Astronomy, Tel Aviv University, Tel Aviv 69978, Israel
[24]International Centre for Elementary Particle Physics and Dept of Physics, University of Tokyo, Tokyo 113, and Kobe University, Kobe 657, Japan
[25]Brunel University, Uxbridge, Middlesex, UB8 3PH UK
[26]Nuclear Physics Department, Weizmann Institute of Science, Rehovot, 76100, Israel
[27]Universität Hamburg/DESY, II Inst für Experimental Physik, 2000 Hamburg 52, Germany
[28]University of Victoria, Dept of Physics, P O Box 3055, Victoria BC V8W 3P6, Canada
[29]University of British Columbia, Dept of Physics, 6224 Agriculture Road, Vancouver BC V6T 1Z1, Canada
[30]University of Oregon, Dept of Physics, Eugene, Oregon 97403, USA

[a]Also at TRIUMF, Vancouver, Canada V6T 2A3
[b]Now at Centre de Physique des Particules de Marseille, Faculté des Sciences de Luminy, Marseille
[c]On leave from Birmingham University, Birmingham B15 2TT, UK
[d]Now at Dipartimento di Fisica, Università della Calabria and INFN, 87036 Rende, Italy
[e]And IPP, McGill University, High Energy Physics Department, 3600 University Str, Montreal, Quebec H3A 2T8, Canada
[f]Also at Shinshu University, Matsumoto 390, Japan

1 Introduction

Measurements of production rates of identified particle species in Z^0 decays are important in providing useful information to test models of parton fragmentation, and should lead to a better understanding of the hadronisation processes. Given sufficient data, the production of individual particle types may be measured separately in quark and in gluon jets and further information obtained to help elucidate the fragmentation schemes. In the context of the Lund string model [1], a general study of observed particle rates provides direct information about such parameters as the vector to scalar ratio in fragmentation, the suppression factor for strange quark pair production, and the probability to form a diquark. Resonant states are particularly interesting because they are less likely than the lighter hadrons to be products of particle decays, so that their dynamics will be generally more closely related to those of the fragmenting partons.

Many particle species have been measured in e^+e^- annihilations at lower energies (a review may be found in [2]), and a number of Monte Carlo programs based on QCD have been tuned so that the measured rates were reproduced. However, many resonant states were measured with poor statistical precision and there were, in addition, some considerable systematic disagreements among experiments. Detailed results on measurements of neutral vector mesons at Petra and PEP may be found in [3], [4], [5], [6], [7] and [8]. The LEP data hold the promise of much better statistical and systematic accuracy than previously available data, and the relative increase in the number of resolvable multi-jet events at LEP energies will enable detailed studies of the differences in particle content between quark and gluon jets.

So far, LEP data have been analysed for inclusive production of various mesons and baryons, including K^0_S [9], π^0 [10], η and $\eta'(958)$ [11], and charged $K^*(892)$, Λ and Ξ [12]. This paper presents some results of a study of neutral vector meson production using a sample of 147k multihadronic decays of the Z^0 taken during 1990 at the OPAL experiment at LEP. The neutral $\rho(770)^0$, $K^*(892)^0$ and $\phi(1020)$ vector meson states have spin-parity $J^{PC} = 1^{--}$, are in the same nonet of $SU(3)_F$ and have similar masses. Thus a comparison of their production rates is particularly useful since many kinematic and dynamical factors may be common to all of them. Direct comparisons may also be made with rates for related particle species such as other vector mesons, and pseudoscalar and tensor mesons.

Ionisation measurements in the OPAL jet chamber permit separation of pions and kaons over a wide kinematical range, allowing the vector mesons to be identified in inclusive two-particle mass spectra via their decay modes: $\rho(770)^0 \to \pi^+\pi^-$, $K^*(892)^0 \to K^\pm\pi^\mp$ and $\phi(1020) \to K^+K^-$. The $K^*(892)^0$ and $\phi(1020)$ resonances appear cleanly in the mass spectra and cross sections have been determined for momenta right up to the kinematical limits. However the $\pi^+\pi^-$ mass spectra show significant momentum-dependent distortion of the resonance lineshape for the $\rho(770)^0$, making it difficult to extract reliable production rates.

2 The OPAL detector

A complete description of the OPAL experiment is given in [13]. For the present analysis, only the information from the central tracking chambers was required, although other parts of the apparatus contributed to the trigger. During the 1990 running, these central chambers surrounded a LEP beam pipe of carbon fibre composite epoxied on a thin aluminium tube of outer radius about 8 cm. The innermost tracking device was the vertex detector, a 1 m long, 470 mm diameter drift chamber which

measures track positions in the $r-\phi$ plane with an accuracy of order 50 μm (in OPAL, the z-axis is defined along the beam direction, and r and ϕ are the usual cylindrical polar coordinates). The jet chamber surrounds the vertex detector and has a sensitive volume of length 4 m with outer and inner diameters of 3.7 m and 0.5 m respectively. The chamber has 24 sectors each containing 159 sense wires parallel to the beam direction, staggered by ± 100 μm either side of a radial plane of potential wires. Space points are formed using the wire position, the ionisation drift time and the ratio of integrated charges measured at the two ends of the wire. The sum of these charges is a measure of ionisation energy loss in the chamber gas. Tracks emerging from the barrel region of the jet chamber, with polar angles between 44° and 136°, have their z-positions accurately measured in a system of drift chambers (the z-chambers) with an efficiency of typically 80% depending on track momentum and direction; these measurements provide precise information on the polar angles of the tracks and are important in improving the resolutions on invariant mass determinations. The potential number of dE/dx samples in the jet chamber is maximal in this angular range. An axial magnetic field of 0.435 T is produced by a warm coil solenoid which surrounds the central detectors. With this field, the momentum resolution, σ_p/p, of the jet chamber is typically $\sqrt{(0.018p)^2+0.02^2}$ (with p in GeV/c) for tracks in multihadronic events. The two-particle mass resolution, σ_M, of the entire tracking system for ϕ, K^* and ρ^0 is 2 MeV, 5.5 MeV and 7.5 MeV respectively at low momentum, and rises to 3.5 MeV, 9 MeV and 13 MeV respectively at the highest momenta.

Particle identification is achieved by using the measurements of specific ionisation energy loss, dE/dx, in the jet chamber gas. The design, construction and operation of the jet chamber is described in detail in [14], and the measurement of dE/dx in [15]. The chamber was run with a gas mixture of 88.2% argon, 9.8% methane and 2% isobutane, and the operating conditions were chosen to be 4 bar gas pressure, 890 Vcm^{-1} drift field and gas gain of about 10^4, in order to provide an acceptable compromise between particle identification by dE/dx and the best z resolution. With these operating conditions the energy loss at minimum ionisation was 7.0 keV cm^{-1}, and a resolution of typically 5.5% was obtained on the dE/dx measurement of a track in a multihadronic event. For a track with the maximum number of hits, the dE/dx resolution was 4.2%.

Figure 1 shows the distribution of measured energy loss against momentum for a sample of 30000 tracks in multihadronic Z^0 decays, selected as described in section 3 below. The main bands in the figure are due to electrons, pions, kaons and protons as indicated; the muon band is very close to the pions, and on the full track statistics a band due to deuterons, mainly from interactions in the beam pipe, is also visible. For each track a χ^2-probability may be evaluated, using the measured momentum and energy loss with their associated errors, indicating the degree to which the particle type is consistent with each of the electron, muon, pion, kaon and proton hypotheses.

3 Data selection

The aim of the event selection procedures was to isolate a clean sample of well measured multihadronic Z^0 decays which could be well simulated by Monte Carlo programs. In the 1990 LEP run, OPAL recorded approximately 147,000 multihadronic events with the central tracking chambers fully operational. From this sample, events were selected which had at least five fitted charged tracks satisfying certain quality criteria: a measured distance of closest approach to the origin of less than 5 cm in the xy-plane and 40 cm in the z direction, a minimum transverse momentum (transverse to the beam direction) of 0.15 GeV/c, a polar angle between 21.6° and 158.4° and at least 20 jet chamber hits. Events passing these selections were then tested for energy and momentum balance, and were rejected if the total visible energy carried by charged tracks (assuming all tracks to be pions) was less than 20%, or the magnitude of the total reconstructed momentum vector was larger than 40%, of the

centre-of-mass energy. A total of 133039 events remained after these cuts. Subsequently only well measured tracks of momentum above 0.25 GeV/c, with $|\cos\theta| < 0.72$ and with associated z-chamber hits, were used in making the mass spectra. On average there were 11.05 such well measured tracks per selected event.

4 Monte Carlo simulation

A sample of 164042 multihadronic Z^0 decay events was generated by the Lund Monte Carlo program Jetset72 [16] (employing parton showers and string fragmentation) and was passed through a full simulation of the experiment [17] and the reconstruction and analysis programs. The initial parton configuration in the simulated events followed the expectations of the Standard Model, and the produced resonances had no preferred spin alignment (which was found for the vector mesons to be in accord with the data within statistics). This event sample served both as a model of the real experimental data, and as a means of measuring the acceptance and efficiencies of the experiment and the data analysis procedures. As a model of the data, the parameters of Jetset were tuned [18] so that the program reproduced many global features of multihadronic events as observed at LEP; the parameters controlling the particle composition of jets, such as the vector to pseudoscalar ratio and the strange quark suppression factor, were kept as the default values based on observed particle production rates at lower energy e^+e^- colliders; the option to simulate Bose-Einstein effects in the final state was not selected.

After the event selection cuts, as described in the previous section, 151413 Monte Carlo events remained, and an average of 12.43 tracks per selected event passed the final track selection criteria. In order to make direct comparisons between the Monte Carlo and real data, the samples were normalised to the same number of multihadronic events after the event cleaning cuts. Well understood shortcomings in the simulation of the matching of jet chamber tracks to z-chamber hits accounted for the discrepancy in mean numbers of well measured tracks in the real and simulated data samples. To allow for this, each track in the Monte Carlo sample was given an additional weight which was a function of its transverse momentum and polar angle, and two-particle combinations were entered in histograms with the product of the two weights. These additional weights varied between 0.78 and 1.05 with a mean value of 0.89; the uncertainty in these track weights was about 1% and was included in later determinations of the systematic errors.

In the processing of the Monte Carlo data sample, information about the true source of each track in the simulated events was preserved, so that at the final analysis stage the various components contributing to two-particle mass spectra could be identified and treated separately. These components of the Monte Carlo spectra were later used in fits to the data.

An additional sample of 96137 events was generated by the Monte Carlo program Herwig [19] and was used for checks on possible systematic effects in the analysis arising from the use of Jetset as a model of the real data. Hadrons in Herwig come from decays of rather low mass clusters and relative particle abundances are determined mainly by phase space. On the other hand the hadrons in Jetset are produced within the Lund string model with rates largely determined by phenomenological parameters.

5 Particle identification

5.1 The particle identification algorithm

For particle identification, each track was required to have at least 20 hits used for dE/dx measurement (a jet chamber hit was used as long as there was no other hit within 1 cm) and to have a measured energy loss of less than 40 keV cm^{-1}, above which the Monte Carlo simulation was unreliable. The mean multiplicity per event was 10.45 such tracks in selected real data events and 10.54 weighted tracks in the Monte Carlo events. Figure 1 shows that the particle separation capability of the dE/dx measurements depends in a rather complex way on track momenta, as the various bands overlap in different momentum regions. The broad spread of high-momentum tracks away from the main bands with measured dE/dx around 16 keV cm^{-1} is caused by unresolved overlapping tracks, leading to a dE/dx measurement of about twice that expected for a single track. This effect is well reproduced by the Monte Carlo simulation, as are all other detailed features of figure 1.

For the particle identification in the present analysis, the list of particle types considered varied with momentum range. From 0.25 to 0.8 GeV/c the four types, e, π, K and p were allowed; from 0.8 to 1.25 GeV/c, e, π and p were allowed; from 1.25 to 2 GeV/c only e and π were considered; and from 2 GeV/c up to 45 GeV/c only π and K were allowed. Thus $e^{\pm}$ could be identified from 0.25 to 2 GeV/c, $\pi^{\pm}$ from 0.25 to 45 GeV/c, $K^{\pm}$ from 0.25 to 0.8 GeV/c and from 2 to 45 GeV/c, and $p/\overline{p}$ from 0.25 to 1.25 GeV/c.

The low momentum limit for particle identification was put at 0.25 GeV/c since below this level the dE/dx has little discriminating power between pions and electrons, while kaons and protons give energy loss values above 40 keV cm^{-1}. In the low momentum range, the e and K bands overlap around 0.6 GeV/c and, since electrons from γ conversions are important at low momenta, there is some contamination of the K sample between 0.55 and 0.7 GeV/c. At 0.8 GeV/c the K band begins to overlap the π band, and since pions are expected to outnumber kaons by a factor of about 10, the K hypothesis is not considered further until the K band begins to emerge again at around 2 GeV/c. Thus the kaon tracks will here contaminate the pion sample. For momenta greater than 1.25 GeV/c the proton band is considered to be too close to first the pion band, and then the kaon band. Therefore protons are no longer considered in the identification, and the protons here give some contamination of the π and K samples. Although the proton band separates again above about 6 GeV/c, the rate of proton production relative to that for kaons is low and attempting to identify protons would result in a considerable loss of kaons. Above 2 GeV/c the K band is well enough separated again from the π band to allow positive identification of kaons. Since the electron and pion bands begin to merge above 2 GeV/c, the electrons are no longer considered because their rate relative to pions is low.

For a track to be positively identified as a specific type, the corresponding χ^2-probability of the dE/dx–momentum measurements was required to be greater than 5% and had to be larger than the probabilities for each of the other hypotheses considered. An average of 9.50 tracks per real event and 9.72 weighted tracks per simulated event had a definite particle type assignment. This small 2% difference, between data and simulation, in numbers of identified tracks could be due either to genuine differences in the physics of the event samples or to failures of the simulation properly to represent the detector (or a combination of both); thus half of this difference was corrected for by applying a further normalisation factor in the Monte Carlo sample and the uncertainty was taken into account in the later evaluation of the systematic errors in the particle production rates.

5.2 Identification efficiencies

The Monte Carlo tracks have been used to measure the momentum-dependent particle identification efficiencies and the purities of track samples, and the resulting distributions are shown for pions and kaons in figures 2(a-d). The values plotted are partial efficiencies based on the starting sample of well measured tracks with at least 20 dE/dx hits and an energy loss below 40 keV cm^{-1}. The distributions are given separately for momenta below 2 GeV/c and for the range 2 to 40 GeV/c. The detailed behaviour of the efficiencies and purities may be understood with reference to figure 1 and the particle identification algorithm: as bands cross in the dE/dx–momentum plot the relevant efficiencies and sample purities fall. Up to 2 GeV/c the pion identification efficiency is close to the maximum possible 95% (based on a cut at 5% χ^2-probability); the efficiency falls from 85% at 2 GeV/c, where kaons are again allowed to be identified, to 65% at 40 GeV/c. The purity of the pion sample varies from 96% at 0.5 GeV/c to 70% at high momentum. There is no attempt to identify kaons from 0.8 to 2 GeV/c causing the step down in pion sample purity at 0.8 GeV/c. In the low momentum range, 0.25–0.8 GeV/c, the kaon efficiency and purity are high except where the electron band crosses, when both fall to around 50%. The kaon identification efficiency is 85% at 2 GeV/c, and falls to about 65% at 40 GeV/c. The kaon purity in this higher momentum region is relatively constant at 45% except near 2 GeV/c where it falls to 35%.

Because no kaons are identified for momenta between 0.8 and 2.0 GeV/c there is no acceptance for $\phi(1020)$ over a momentum range from 2.2 to 3.2 GeV/c. This excluded region for the $\phi(1020)$, corresponding to $0.04 < x_p < 0.08$, is relatively small, and it is implicitly assumed in the further analysis that the Monte Carlo simulation gives an accurate model of the behaviour, but not the absolute rate, of $\phi(1020)$ production over a range of momentum which includes this region. On the other hand, Monte Carlo studies have shown that, because of the larger momentum of the K^* decay products in the K^* rest system, the $K^*(892)^0$ acceptance is non-zero over the entire momentum range above 0.25 GeV/c despite the limitations on the accepted laboratory kaon momenta.

5.3 Independent checks of dE/dx performance

In order to study further the accuracy of the simulation of particle energy loss, track samples were obtained from both the real and the Monte Carlo data for electrons, pions and protons using identification methods independent of dE/dx. Pions were obtained from well reconstructed K^0_S decays, protons from Λ particles, and electrons were flagged using electromagnetic calorimetry. Although these track samples were somewhat different in character from the tracks used in the vector meson analysis, they were nevertheless useful in verifying many aspects of the dE/dx simulation and in giving further confidence in the analysis. Additional sets of electron, pion, kaon and proton tracks were obtained from the Monte Carlo data using the generator level information to identify the tracks, and these samples corresponded in character to the tracks used in the vector meson analysis. All of the selected track samples were subjected to the same cuts as used in the physics analysis and were processed by the dE/dx identification algorithms described above.

This exercise permitted studies of deviations, in the relativistic rise region, between the measured average energy losses for each particle type and the values, <dE/dx>, assumed in the calculations of the χ^2-probabilities in the initial data processing. Small (of order 2%) corrections to these assumed mean values were found to be needed in both real and simulated data. The corrections required for the Monte Carlo samples obtained using generator level information were found to be the same as for the independently identified Monte Carlo tracks. The values of the measured shifts in the real data for e, π and p were used to infer, by interpolation, the likely shift for the kaons together with its uncertainty,

and this interpolation procedure was verified by applying it to Monte Carlo samples identified using the generator information. Distributions of weighted deviations ((dE/dx−<dE/dx>)/$\sigma_{dE/dx}$) next gave information about the accuracy of the dE/dx measurement errors, $\sigma_{dE/dx}$. These distributions had means of zero and unit widths for the Monte Carlo track samples, but for the real data an overall factor of 1.025 multiplying the errors was required to obtain unit widths. The distributions of measurement errors were then compared between the data and Monte Carlo, and a global factor of 1.05 multiplying the Monte Carlo values brought the two distributions into line. Figure 3 shows a comparison between the data and the simulation in the final distribution of resolution on the dE/dx measurements, $\sigma_{dE/dx}$, for the pion tracks from K^0_S decays; it is apparent that the simulation gives an excellent representation of the behaviour of the real tracks.

Efficiencies and misidentification probabilities were then computed independently for the real data and for the Monte Carlo track samples as functions of momentum, using the knowledge of particle type obtained from topology or calorimetry. Table 1 gives ratios of simulation to data for pion identification efficiencies and misidentification probabilities and indicates only small differences between real data and Monte Carlo.

For the physics analysis, the results of these studies were used in recalculating the χ^2-probability values for both the data and the Monte Carlo tracks before application of the particle identification algorithms detailed above, and all the uncertainties in the corrections were taken into account in later evaluation of systematic errors in particle rates (this will be discussed further in section 7.3).

6 Two-particle mass spectra

6.1 Kπ and KK mass spectra

Two-particle mass spectra were compiled for various ranges of the scaled momentum variable x_p, given by

$$x_p = p/E_{beam} = 2p/\sqrt{s},$$

where p is the total momentum of the 2-particle combination, E_{beam} the beam energy and $\sqrt{s}$ the total centre-of-mass energy. The data were divided into 5 bins of x_p for Kπ and 3 for KK, and the spectra were computed for all combinations of same charge and opposite charge for each of Kπ and KK. Figures 4(a-b) show the overall mass spectra, integrated over x_p, for $K^{\pm}\pi^{\mp}$ and K^+K^-. The points with error bars are the OPAL data and the solid histograms show the Jetset72 predictions with the simulated data analysed in the same way as the real data; the Monte Carlo sample has been absolutely normalised to the same total number of multihadronic Z^0 decay events as the real data sample, taking full account of all weighting factors discussed previously. For comparison, figures 4(c-d) show the corresponding like-sign mass spectra for $K^{\pm}\pi^{\pm}$ and $K^{\pm}K^{\pm}$.

'Background-corrected' mass spectra were obtained by bin-by-bin subtraction of like-sign spectra from those for the neutral charge combinations. Several drawbacks are associated with this background subtraction technique. For example it is likely that dynamical effects from decays of higher mass resonances will result in differences in the non-resonant contributions to the like-sign and unlike-sign mass plots. Also, as will be discussed below, Bose-Einstein correlations may produce low mass enhancements in like-sign spectra which would affect only indirectly the spectra for oppositely charged pairs, so that the like-sign spectra may not be a good approximation to the non-resonant unlike-sign ones, especially at low mass. However, the aims here were to measure the intensities of the resonances in the mass spectra rather than study the detailed shapes of the backgrounds, and the final analysis

was relatively insensitive to the precise procedures used to obtain the mass plots. What was required were large reductions of the combinatorial backgrounds with relative enhancements of the resonance signals. These criteria were found to be well satisfied by the procedures used. The resulting overall 'background-subtracted' spectra are shown for both data and Monte Carlo in figures 4(e-f).

It is clear from figure 4 that the shapes and absolute levels of the background-subtracted $K^{\pm}\pi^{\mp}$ and $K^{+}K^{-}$ spectra are rather well simulated by Jetset72 even though there are some discrepancies in the raw plots. However there are clear disagreements in the intensities of the resonance signals for $K^{*}(892)^{0}$ and $\phi(1020)$. In the case of the $K^{*}(892)^{0}$ care is needed in the interpretation of any discrepancy since the reflection from the $\rho(770)^{0}$ is important. The $K^{\pm}\pi^{\mp}$ data, figure 4(e), show additionally an indication for production of the tensor meson, $K_2^{*}(1430)$, which, with the current parameter set, is not included in the Jetset fragmentation scheme and so is not seen in the simulation.

Because of the inherent limitations of the particle identification procedures, the $K^{\pm}\pi^{\mp}$ and $K^{+}K^{-}$ mass spectra have many entries from wrongly identified particle pairs, and in particular from cases where both tracks are pions. Resonances in particular channels appear also as (lower intensity) reflections in other channels. The relative intensities of the signals and reflections vary with the momenta of the tracks, and so with the x_p of the resonances, as identification efficiencies and sample purities change. As discussed in section 5, these effects are well understood and well reproduced by the simulation. Significant contributions to the $K\pi$ mass spectra arise from $\rho(770)^{0}$ and Λ, with lesser effects due to $\phi(1020)$, $\omega(783)$, K^{0}_{S}, η, $\eta'(958)$ and $\gamma \rightarrow e^{+}e^{-}$. Figure 5(a) shows how the ρ^{0} and Λ reflections contribute to the overall background-subtracted Monte Carlo $K^{\pm}\pi^{\mp}$ mass spectrum of figure 4(e). The unshaded portion of the plot arises from uncorrelated particle pairs and the other minor contributions.

6.2 $\pi\pi$ mass spectra

The $\pi\pi$ mass spectra have been treated in the same way as described above for $K\pi$ and KK, and the corresponding spectra are shown in figures 6(a-c); marked differences are apparent between the data and the Monte Carlo. These differences are in large part due to Bose-Einstein correlations which are present in the data [20]; these correlations can result in an enhancement in the number of like-sign pion pairs at low mass with a reduction in the number at higher masses. In the main Monte Carlo production the option to select Bose-Einstein effects was not used. Figures 6(a-c) show that the Monte Carlo simulation is poor at low mass, below 0.4 GeV, where Bose-Einstein effects may be expected to be strongest in the $\pi^{\pm}\pi^{\pm}$ spectra and the effects of η and η' production are important in the $\pi^{+}\pi^{-}$ spectra. However at higher masses, and notably in the region of the ρ^{0} meson, there are also significant differences between the data and the simulation. In particular, the peak position for the ρ^{0} appears shifted to lower mass in the real data. Additionally the resonance signal is somewhat smeared out. Since the mass resolution of the experiment is much less than the ρ^{0} width, this cannot account for the observations.

A good understanding of the $\rho(770)^{0}$ is important for the measurement of $K^{*}(892)^{0}$ rates because the ρ^{0} reflects into the $K\pi$ mass spectra, appearing at a similar mass as the K^{*} signal and having a shape in its reflection which depends on its true shape in $\pi^{+}\pi^{-}$. For the Jetset simulation, all meson resonances are treated as having simple non-relativistic Breit-Wigner shapes which add incoherently with the background. The $\rho(770)^{0}$ is well known to have a rather different behaviour in the way it manifests itself in $\pi^{+}\pi^{-}$ mass spectra (see [21] for a review). A more correct representation of the resonance shape would be by a relativistic p-wave Breit-Wigner with a mass-dependent width [22]; even this shape has been seen to be considerably distorted in various experiments [23], possibly by a

mechanism involving interference with a coherent p-wave $\pi^+\pi^-$ background [24]. However these effects are small compared to the discrepancies between Monte Carlo and data in figures 6(a) and 6(c).

Figure 5(b) shows the main components making up the background-subtracted Monte Carlo mass spectrum of figure 6(c). It can be seen that below 0.4 GeV large contributions arise from decays of η and $\eta'(958)$ mesons to states containing $\pi^+\pi^-$ and neutral particles; it is now established [11] that Jetset with default parameters produces η' mesons at too high a rate. The mass region between 0.4 and 0.6 GeV is dominated by the effects of $\omega(783)$ and K^0_S production. It seems possible that a proper understanding, and a good simulation, of the Bose-Einstein correlations, taken together with independent measurements of η, η' and K^0_S rates, could allow useful information to be obtained on the rate of $\omega(783)$ production via the effects on the low-mass $\pi^+\pi^-$ mass spectra.

6.3 Bose-Einstein effects

To investigate the possible effects of Bose-Einstein correlations on the 2-particle mass spectra, a reweighting technique was used (because of the impracticality of reprocessing the full Jetset Monte Carlo data samples through the entire production chain). In the reweighting, each entry in the Monte Carlo mass spectra was assigned a weight dependent on the Jetset generator-level properties of the particular particle pair. To compute these weights, two-dimensional histograms of mass versus x_p were produced using Jetset for each of $\pi\pi$, Kπ and KK, and for all 2-particle charge states, with entries being made only when neither particle came directly or indirectly from the decay of a long-lived state (of width smaller than 20 MeV). Three runs of Jetset were made: the first, run 1, had no Bose-Einstein effects included; the second, run 2, used the Jetset Gaussian parametrization of Bose-Einstein correlations for all pions and kaons (MSTJ(51)=2, MSTJ(52)=7) with default values for the strength (PARJ(92)=1.) and the region size (PARJ(93)=0.2 GeV); the third, run 3, again used the Gaussian parametrization but with the parameter values obtained in fits [20] to the Bose-Einstein correlation function in the OPAL data (MSTJ(51)=2, MSTJ(52)=9, PARJ(92)=2.5 and PARJ(93)=0.33 GeV). Two dimensional histograms of weights were then obtained by dividing the histograms of mass versus x_p, produced in each of the Jetset runs 2 and 3, by those obtained in run 1 with no Bose-Einstein effects included. The production Monte Carlo data were then reanalysed, with these histograms being used to obtain weights for every particle pair, using the known generator-level properties of each track. If either track of a pair came from a long-lived state or was of a type other than pion or kaon, then no additional weight was applied. Thus new sets of two-particle mass spectra were obtained weighted for the effects of Bose-Einstein correlations. This procedure was verified by computing the Bose-Einstein correlation function for the real data and comparing with the reweighted Monte Carlo production data using the weights obtained from Jetset run 3. Good agreement was obtained with the results of [20].

The reweighted mass spectra for Kπ and KK were found to be only slightly different from those of figure 4. In particular the inclusion of the Bose-Einstein effects (shown, for the OPAL parameters, as the dotted histograms in figures 4(b) and 4(d)) accounts for less than half of the discrepancy between data and Monte Carlo in the raw KK mass spectra at masses below 1.1 GeV. However, the $\pi\pi$ mass spectra changed significantly with the inclusion of the Bose-Einstein correlations. Figure 6(d) shows the background-subtracted $\pi^+\pi^-$ mass spectrum for the real data (points) compared with the Jetset prediction reweighted according to the output of run 2 (default Bose-Einstein parameters). Figure 6(e) shows the results of run 3, using the OPAL parameter values. It can be seen that the apparent position of the ρ^0 meson peak in the subtracted mass spectra shifts significantly between figures 6(c,d and e), while the low mass region also changes. No one simulation provides a good description of the entire mass spectrum. The good agreement between data and simulation for masses above 0.5 GeV in figure 6(e) indicates the importance of the Bose-Einstein effects in the Jetset simulation of the $\pi\pi$

mass spectra. On the other hand, there is disagreement in the raw (unsubtracted) $\pi\pi$ mass spectra, and a full understanding requires further study. The apparent shift in mass of the ρ^0 peak position in the subtracted spectrum is partly an artefact of changes in the shapes of the non-resonant $\pi^{\pm}\pi^{\pm}$ and $\pi^+\pi^-$ backgrounds, and is partly due to a genuine shift of the ρ^0 peak induced when the Bose-Einstein effects are switched on in Jetset. It is interesting to note that Bose-Einstein correlations within the framework of Jetset can have quite significant effects on the mass distribution of $\pi^+\pi^-$ systems, and that these effects are such as to improve the agreement with the real data. The changes to $\pi^+\pi^-$ spectra are possibly an indirect consequence of the effect on $\pi^{\pm}\pi^{\pm}$ systems and the proximity in phase space of a relatively large number of pions.

Because of the uncertainty in the true distributions of the components of the $\pi\pi$ mass spectra, reliable measurements of $\rho(770)^0$ production cannot be made at present and require further study. However the effects of Bose-Einstein correlations on KK and Kπ mass spectra are sufficiently small that the systematic errors from this source on measurements of $\phi(1020)$ and $\mathrm{K}^*(892)^0$ are significantly less than the statistical errors. Thus the uncertainty due to these effects does not preclude reliable measurements of the ϕ and the K^* mesons.

7 Fits to the two-particle mass spectra

In order to extract production cross sections for the $\phi(1020)$ and $\mathrm{K}^*(892)^0$ vector mesons, weighted least-squares fits have been made to the appropriate mass spectra, binned for two-particle combinations in the various ranges of x_p. In the Jetset Monte Carlo event sample, information was available about the source of each track at the generator level and these events provided the detailed shapes and predicted intensities of each of the possible components of the mass spectra, including the resonance signals and all reflections, in each of the x_p bins. These separate components of the Monte Carlo two-particle mass spectra were used directly, without parametrization, as inputs to the fits to the spectra of the real data. This direct use of the detailed Monte Carlo shapes automatically accounted for any momentum dependent changes in signal shapes, backgrounds and reflections. Since the simulated data were absolutely normalised to the same effective number of Z^0 decays as the real data, the results of the fits gave directly the measured ratios of real data to Jetset intensities for each of the components of the mass spectra. Multiplicities and normalised differential cross sections (fragmentation functions) were then obtained by appropriately scaling those assumed by Jetset.

7.1 Fits to the $\mathrm{K}^+\mathrm{K}^-$ mass spectra

The $\mathrm{K}^+\mathrm{K}^-$ data were binned in 3 ranges of x_p, and the corresponding background-subtracted mass spectra are shown as the data points with error bars in figure 7. The $\phi(1020)$ is a narrow state, close to threshold, is well separated from all possible contaminating channels and can be interpreted without detailed reference to reflections from other resonances. As figure 4(f) shows, the general shape and level of the background is well reproduced by the Monte Carlo but there is clear disagreement in the magnitude of the signal. Fits to the experimental data in the three x_p bins have been made, over the mass range up to 1.06 GeV, using the shapes for the ϕ and the backgrounds as obtained from the simulation. The fits were sensitive only to variations in the intensities of the ϕ and the $\mathrm{K}^+\mathrm{K}^-$ non-resonant background and so only these were varied in the final fits; all other Monte Carlo components were small and were fixed at their default Jetset values. The solid histograms in figures 7(a-c) show the results of the fits, and the χ^2 values are listed in table 2.

The measured $\phi(1020)$ rates are given in table 2 as multiplicities and as normalised differential cross sections, $1/\sigma_{had}.\mathrm{d}\sigma/\mathrm{d}x_p$, for each of the bins of x_p. Here σ_{had} is the total cross section for hadronic Z^0 decay. The overall multiplicity was measured to be $0.085 \pm 0.015 \pm 0.010$ $\phi(1020)$ mesons per hadronic Z^0 decay over the x_p range 0.01–1.0. According to both Jetset 7.2 and Herwig 5.0, the correction to this figure from the unobserved region below $x_p = 0.01$ adds an almost negligible amount. The statistical errors given are those obtained from the fits and include contributions from the Monte Carlo as well as the real data statistics; smaller systematic errors (to be discussed below) arise from uncertainties in the dE/dx, the normalisation of the simulation, the mass resolution of the experiment, the branching ratio of ϕ to $K^+K^-$and the effects of Bose-Einstein correlations. In order to obtain the appropriate value of x_p within a given bin, for which to quote the measured cross section, the Jetset x_p-dependence has been assumed. The fragmentation functions are shown in figure 9(a) in comparison with the predictions of default Jetset 7.2 (solid line), Herwig 5.0 (dotted line) and Jetset tuned (dashed line), as described below in section 8, to reproduce a number of measured multiplicities.

7.2 Fits to the $K^{\pm}\pi^{\mp}$ mass spectra

The mass range for fitting to the $K^{\pm}\pi^{\mp}$ spectra was chosen as 0.64–1.2 GeV and the data were binned in 5 ranges of x_p. The intensities of the $\phi(1020)$ were fixed at the levels obtained in the earlier fits while those due to contributions other than the $K^*(892)^0$ and the non-resonant $K\pi$ backgrounds were fixed at their Jetset values. In the case of the $K^*(892)^0$ the natural width is small enough, at 50 MeV, that a simple Breit-Wigner peak as used by Jetset gives a good representation of the resonance shape in the data, as figure 4(e) indicates. All fits behaved well and produced χ^2 values, given in table 3, which indicated that the models were providing a good description of the data. Figures 8(a-e) show the fitted mass spectra in the 5 ranges of x_p.

The measured $K^*(892)^0$ multiplicities and differential cross sections are given in table 3. The quoted systematic errors are dominated by uncertainties in the shape and intensity of the ρ^0 reflection (including effects of Bose-Einstein correlations), but include also uncertainties in the normalisation of the Monte Carlo simulation and in the performance of the dE/dx procedures. The overall multiplicity has been measured to be $0.755 \pm 0.067 \pm 0.060$ $K^*(892)^0$ per multihadronic Z^0 decay. In correcting the observed multiplicity for the very low x_p region, the Jetset behaviour of the rate has been assumed; however, as table 3 shows, the additional contribution is negligible within the measurement errors, and the uncertainty in the extrapolation is also negligible compared to the other systematic errors. The fragmentation function is shown in figure 9(b) where the rates are compared to the default Jetset 7.2, Herwig 5.0 and the the tuned Jetset predictions.

7.3 Systematic errors

Table 4 provides a summary of the contributions to the systematic errors on the measured overall $\phi(1020)$ and $K^*(892)^0$ multiplicities. These systematic errors come from a number of sources, many of which have already been discussed. The tables show that the overall systematic errors are a little smaller than the statistical errors and that the systematics are dominated by the mass resolution in the case of the $\phi(1020)$ and by the uncertainty in the Bose-Einsten effects in the case of the $K^*(892)^0$.

All measured rates are subject to errors of $\pm 2\%$ from the normalisation of the simulation, coming partly from the track multiplicity discrepancies mentioned in section 4, partly from the jet chamber to z-chamber matching inefficiencies, and partly from the overall event and track cuts (as studied using

event samples produced by both Jetset and Herwig). The error from the particle data tables on the branching ratio $\phi(1020) \rightarrow K^+K^-$ was included as a systematic error on the measurements of ϕ rates.

Two main sources of systematic uncertainty were present in the particle identification: the position of the theoretical average energy loss curve for kaons, and the possible small discrepancies between data and simulation in overall performance of the algorithms. To determine the systematic errors due to these factors, the data were reanalysed for different assumptions based on the studies described in section 5.3, and all of the fits were repeated. The total rate for $\phi(1020)$ varied by typically 6% and that for $K^*(892)^0$ by 3%, well within the statistical errors.

Since the ϕ is a narrow state, possible discrepancies between the data and the simulation in the mass resolution could contribute to systematic effects. To investigate this, the real and Monte Carlo mass spectra were fitted independently to sums of polynomials and Gaussian peaks. The resulting widths, σ_M, were compatible between the two data sets although the errors on the widths were significantly larger for the real data. The real data spectra were then fitted using values of σ_M fixed at ± 1 standard deviation away from the values obtained in the free fits. It was found that the intensity of the ϕ meson peak varied by $\pm 8\%$ and this was taken as the appropriate contribution to the systematic errors on the measured $\phi(1020)$ rates. A small correction of 5% was applied to all ϕ rates to account for possible non-Gaussian tails in the real data.

In order to investigate effects on the rates arising from the parametrization and intensity of the $\rho(770)^0$, the fits were repeated using a p-wave Breit-Wigner shape and also with the intensity of the ρ^0 fixed at 0.7 and 1.3 times its assumed Jetset value. No significant changes were made to the rates for the $\phi(1020)$ but there were small variations in the the fitted $K^*(892)^0$ rates, which were taken as the systematic errors arising from these sources.

All of the fits were repeated using the sets of Monte Carlo data reweighted to account for the possible effects of Bose-Einstein correlations. Thus two further sets of fits were made, one for each of Jetset runs 2 and 3 as described in section 6.3. The $\phi(1020)$ rates were found to vary by only a small amount while larger changes ocurred in the fitted $K^*(892)^0$ rates for all of the x_p bins, mainly as a result of variations in the shape and intensity of the $\rho(770)^0$ reflection. The magnitude of these changes in the rates was taken as an indication of the level of the systematic errors arising from this source. In all cases these variations in the fitted rates were significantly smaller than the statistical errors.

In computing the overall multiplicites by adding the rates in each x_p bin, the errors due to each systematic source were combined assuming complete correlation from bin to bin. The final overall systematic errors were then obtained by adding all contributions in quadrature.

8 Discussion and Conclusions

This study of inclusive neutral vector meson production in Z^0 decay has shown a number of unexpected features. First, the shape of the $\pi^+\pi^-$ mass spectrum in the data is distorted in the region of the $\rho(770)^0$ resonance and the peak mass shifted to lower values, especially at low momentum. This differs from previous observations in lower energy e^+e^- interactions [3, 4, 8] where successful fits were obtained to the mass spectra using the standard ρ^0 parameters. The reason for this different behaviour at LEP energies could be an enhancement of the effects of Bose-Einstein correlations arising from the increased multiplicity of pions which are close in phase space to the decay products of the ρ^0. Interference effects between the relatively broad ρ^0 and possible coherent p-wave backgrounds could

also be present. Better modelling of the $\rho(770)^0$ lineshape is an obvious prerequisite to a determination of its production rates in Z^0 decays.

The $K^*(892)^0$ rates measured by OPAL are in good agreement with Herwig 5.0 but significantly below the level of the Jetset 7.2 predictions (see figure 9(b)). The overall multiplicity, measured to be 0.76 ± 0.09 per Z^0 is in accord with the figure of 0.77 given by Herwig while Jetset with default parameters predicts 1.06. It is apparent from figure 4(a), the overall $K^\pm\pi^\mp$ mass spectrum, that Jetset reproduces well the level and shape of the $K^\pm\pi^\mp$ system in the real data, except in clearly overestimating the intensity of the K^{*0} signal. The present result for the K^{*0} rate is lower than a recent result from the DELPHI collaboration [12] for $K^*(892)^\pm$ which quotes an overall rate of 1.33 ± 0.26 per event. The charged K^* multiplicity would be expected to be close to the rate for K^{*0}.

The $\phi(1020)$ results reported here present an additional problem for the Monte Carlo programs, being discrepant with both of the models tested. The measured multiplicity, 0.086 ± 0.017, is in fact similar to the rate obtained in e^+e^- collisions at $\sqrt{s} = 30$ GeV, is less than half of the default Jetset expectation of 0.190, and is also below the Herwig figure of 0.115. The disagreement between Jetset and Herwig, both tuned to overall event shapes, indicates that there is still much uncertainty in the models as to how the multiplicities of specific particle types are determined and how they change with energy.

As mentioned in the introduction, rates for several particle species, as well as the overall multiplicity of charged particles, have now been measured in LEP experiments. Table 5 summarises the measurements to date, listing the multiplicities obtained (over restricted ranges of x_p in cases where significant systematic errors arise from extrapolating into regions of zero acceptance). Up till now the measured rates, apart from that for the $\eta'(958)$, have all been compatible with the default parameter values of Jetset. The strangeness suppression, in particular, has been assumed to be well specified by the rate for K^0 relative to all charged particles. However, to accommodate the measurements of $K^*(892)^0$ and $\phi(1020)$ presented here, it is clear that the default value of 0.3 is too high. In order that Jetset continue to reproduce the measured K^0 multiplicity, any reduction in the value of this strangeness suppression parameter would have to be compensated by an increase in the rate of pseudoscalar meson production relative to vector meson production. A scan has been made of the Jetset parameters which control the strangeness suppression (PARJ(2) with default value 0.3) and the probability that a strange meson will have spin 1 (PARJ(12) with default value 0.6), in order to obtain the best values to reproduce the observations listed in table 5. The rates for η and η' were not included in this tuning procedure because they are likely to be more sensitive to the choice of mixing angle in the $SU(3)_F$ nonet [25, 11]. No single local minimum of the χ^2 was found; various pairs of values in the range 0.23–0.27 for strangeness suppression and 0.4–0.5 for the spin-1 probability gave acceptable fits to the data. For example, values of 0.245 and 0.43 respectively give a χ^2 value of 10.5 for the 8 measurements. This compares with χ^2 values of 55 for Jetset with default parameters and 156 for default Herwig 5.0. Variations of these two Jetset parameters at this level were found to have essentially no effect on the overall event shapes, described in [18], and no changes in the other parameters were needed. The Jetset rates for these parameter values together with the rates from default Herwig 5.0 are listed in the table, and the dashed curves in figure 9 show the resulting fragmentation functions. As may be seen from the table, the largest contribution to the χ^2 comes from the charged $K^*(892)^\pm$ rate measured in [12]. It is worth remarking that D_s decays are a significant source of $\phi(1020)$ mesons especially at large x_p, and inadequate modelling of the production and decay rates in the Monte Carlo could account for some of the discrepancy between data and Jetset.

The tuning of Jetset at this level is purely phenomenological and the PARJ values obtained will be sensitive to assumptions about production rates and decay branching ratios of heavy flavour mesons and baryons. However the exercise is useful in obtaining a better set of parameters for the simulation

of LEP physics, and such a set of has been found to reproduce all the particle rates. However the real emphasis of the present work has been on obtaining accurate values for the multiplicities and fragmentation functions for the neutral vector mesons as part of an ongoing study of particle rates in Z^0 decays. Only with significantly more knowledge of the rates for identified particle species will a consistent picture emerge which, it is to be hoped, will enable a proper understanding of quark and gluon hadronization.

9 Acknowledgements

It is a pleasure to thank the SL Division for the efficient operation of the LEP accelerator, the precise information on the absolute energy, and their continuing close cooperation with our experimental group. The computer centres at CERN and RAL have provided excellent facilities for the data handling and analysis. In addition to the support staff at our own institutions we are pleased to acknowledge the
Department of Energy, USA,
National Science Foundation, USA,
Science and Engineering Research Council, UK,
Natural Sciences and Engineering Research Council, Canada,
Israeli Ministry of Science,
Minerva Gesellschaft,
Japanese Ministry of Education, Science and Culture (the Monbusho) and a grant under the Monbusho International Science Research Program,
American Israeli Bi-national Science Foundation,
Direction des Sciences de la Matière du Commissariat à l'Energie Atomique, France,
Bundesministerium für Forschung und Technologie, FRG,
National Research Council of Canada, Canada,
A.P. Sloan Foundation and Junta Nacional de Investigação Científica e Tecnológica, Portugal.

References

[1] B. Anderson et al.: Phys. Rep. 97 (1983) 31.

[2] W. Hofmann: Ann. Rev. Nucl. Part. Sci. 38 (1988) 279.

[3] TASSO Coll., R. Brandelik et al.: Phys. Lett. 117 B (1982) 135.

[4] JADE Coll., W. Bartel et al.: Phys. Lett. 145 B (1984) 441.

[5] H. Aihara et al.: Phys. Rev. Lett. 52 (1984) 2201.

[6] H. Aihara et al.: Phys. Rev. Lett. 53 (1984) 2378.

[7] M. Derrick et al.: Phys. Lett. 158 B (1985) 519.

[8] S. Abachi et al.: Phys. Rev. D 40 (1989) 706.

[9] OPAL Coll, G. Alexander et al.: Phys. Lett. B 264 (1991) 219.

[10] L3 Coll., B. Adeva et al.: Phys. Lett. B 259 (1991) 119.

[11] ALEPH Coll., D. Buskulie et al.: CERN-PPE/92-74.

[12] DELPHI Coll., P. Abreu et al.: Phys. Lett. 275 B (1992) 231.

[13] OPAL Coll., K. Ahmet et al.: Nucl. Instrum. Methods A 305 (1991) 275.

[14] H. M. Fischer et al.: Nucl. Instrum. Methods A 283 (1989) 492.

[15] M. Hauschild et al.: Nucl. Instrum. Methods A 314 (1992) 74.

[16] T. J. Sjöstrand: Comp. Phys. Commun. 39 (1986) 347;
T. J. Sjöstrand, M. Bengtsson: Comp. Phys. Commun. 43 (1987) 367.

[17] J. Allison et al.: CERN-PPE/91-234, to be published in Nucl. Instrum. Methods A.

[18] OPAL Coll., M. Z. Akrawy et al.: Z. Phys. C 47 (1990) 505.

[19] G. Marchesini, B. R. Webber: Nucl.Phys. B 310 (1988) 461;
G. Marchesini et al.: Cavendish-HEP/90-26 and DESY-91-048, to be published in Comp. Phys. Commun.

[20] OPAL Coll., P. D. Acton et al.: Phys. Lett. B 267 (1991) 143.

[21] For a discussion see meson listings in 1984 Review of Particle Properties, Rev. Mod. Phys., Vol.56, No.2, Part 2, April 1984.

[22] J. D. Jackson: Nuovo Cim. 34 (1964) 1644.

[23] R. J. Apsimon et al.: Z. Phys. C 53 (1992) 581.

[24] P. Söding: Phys. Lett. 19 (1966) 702.

[25] M. Bowler: Phys. Lett. 180 B (1986) 299.

Tables

Momentum range (GeV/c)	Efficiency ratio for π	Misidentification ratio for π to K
0.25 - 0.4	1.030 ± 0.008	1.43 ± 1.22
0.4 - 0.8	1.005 ± 0.004	0.91 ± 0.17
0.8 - 1.0	1.004 ± 0.005	-
1.0 - 1.5	1.003 ± 0.004	-
1.5 - 2.0	0.996 ± 0.003	-
2.0 - 3.0	1.000 ± 0.013	1.01 ± 0.06
3.0 - 5.0	1.028 ± 0.013	0.87 ± 0.06
5.0 - 10.0	1.023 ± 0.021	0.90 ± 0.07
10.0 - 20.0	1.14 ± 0.08	0.70 ± 0.12
20.0 - 45.0	0.83 ± 0.35	1.30 ± 0.84

Table 1. Ratios of efficiencies and misidentification probabilities between simulation and data using pion tracks from K^0_S decays.

Bin	x_p range	$<x_p>$	χ^2/dof	Multiplicity $\phi(1020)/Z^0$ decay	$1/\sigma_{had}.d\sigma/dx_p$
1	0.01 – 0.15	0.10	20.1/20	$0.054 \pm 0.014 \pm 0.006$	$0.39 \pm 0.10 \pm 0.04$
2	0.15 – 0.3	0.22	21.8/20	$0.019 \pm 0.004 \pm 0.003$	$0.12 \pm 0.03 \pm 0.02$
3	0.3 – 1.0	0.45	17.3/20	$0.012 \pm 0.003 \pm 0.001$	$0.017 \pm 0.004 \pm 0.002$
	0.01 – 1.0			$0.085 \pm 0.015 \pm 0.010$	
	0.0 – 1.0			$0.086 \pm 0.015 \pm 0.010$	

Table 2. Measured multiplicities, differential cross sections (fragmentation functions) and fit χ^2 per degree of freedom for inclusive $\phi(1020)$ in multihadronic Z^0 decays. The errors given are statistical and systematic respectively. The value of $<x_p>$ is calculated assuming that the cross section variation over the appropriate x_p range follows that of the Jetset model.

Bin	x_p range	$<x_p>$	χ^2/dof	Multiplicity $K^*(892)^0/Z^0$ decay	$1/\sigma_{had}.d\sigma/dx_p$
1	0.005 – 0.025	0.017	11.5/26	$0.134 \pm 0.018 \pm 0.005$	$6.71 \pm 0.90 \pm 0.23$
2	0.025 – 0.1	0.069	23.4/26	$0.300 \pm 0.058 \pm 0.026$	$4.00 \pm 0.78 \pm 0.34$
3	0.1 – 0.15	0.12	26.6/26	$0.107 \pm 0.017 \pm 0.012$	$2.14 \pm 0.34 \pm 0.24$
4	0.15 – 0.3	0.21	29.4/26	$0.143 \pm 0.017 \pm 0.010$	$0.95 \pm 0.12 \pm 0.06$
5	0.3 – 1.0	0.45	26.4/26	$0.069 \pm 0.012 \pm 0.007$	$0.10 \pm 0.02 \pm 0.01$
	0.005 – 1.0			$0.753 \pm 0.067 \pm 0.060$	
	0.0 – 1.0			$0.755 \pm 0.067 \pm 0.060$	

Table 3. Measured multiplicities, differential cross sections and fit χ^2 values for inclusive $K^*(892)^0$ production.

Error source	Error on $\phi(1020)$ multiplicity	Error on $K^*(892)^0$ multiplicity
Normalisation of MC	± 0.002	± 0.023
Branching ratio	± 0.002	—
dE/dx uncertainty	± 0.005	± 0.019
Mass resolution	± 0.007	—
Intensity of $\rho(770)^0$	—	± 0.019
Bose-Einstein effects	± 0.003	± 0.043
TOTAL	± 0.010	± 0.060

Table 4. Systematic errors on total $\phi(1020)$ and $K^*(892)^0$ multiplicities.

x_p range	Experiment	Particle	Multiplicity	Jetset tuned	Jetset default	Herwig 5.0
0.0 – 1.0	OPAL	all charged	21.40 ± 0.43	21.09	21.35	21.08
0.0075 – 0.065	L3	π^0	6.4 ± 0.4	6.35	6.30	7.02
0.1 – 0.9	ALEPH	η	0.298 ± 0.031	0.34	0.32	0.44
0.1 – 0.9	ALEPH	$\eta'(958)$	0.068 ± 0.024	0.27	0.26	0.12
0.0 – 1.0	OPAL	K^0	2.10 ± 0.14	1.96	2.16	2.12
0.0 – 1.0	OPAL	$K^*(892)^0$	0.76 ± 0.09	0.71	1.06	0.77
0.0 – 1.0	DELPHI	$K^*(892)^\pm$	1.33 ± 0.26	0.75	1.10	0.82
0.0 – 1.0	OPAL	$\phi(1020)$	0.086 ± 0.018	0.115	0.189	0.113
0.01 – 0.2	DELPHI	Λ	0.28 ± 0.02	0.26	0.31	0.36
0.0 – 0.5	DELPHI	Ξ	0.020 ± 0.004	0.019	0.027	0.062

Table 5. Measured multiplicities within specified x_p ranges for identified particles in Z^0 decay, compared with Jetset 7.2 tuned to give best overall agreement (PARJ(2)=0.245, PARJ(12)=0.43) and with Jetset 7.2 and Herwig 5.0 using default parameters. In the tuning, the η and η' rates were not used. The other LEP experiments have also measured the multiplicity of all charged tracks.

Figure Captions

Figure 1. Distribution of dE/dx versus momentum for selected well measured tracks in the real data.

Figure 2. (a) Efficiency of the dE/dx procedures to identify $\pi^{\pm}$, and purity of the $\pi^{\pm}$ sample, both as functions of momentum from 0.25–2.0 GeV/c (the solid squares show efficiency and the triangles indicate the purity); (b) similarly for the momentum range 2.0–40.0 GeV/c; (c) efficiency for $K^{\pm}$ and purity of the $K^{\pm}$ sample for momentum from 0.25–0.8 GeV/c; (d) similarly for the momentum range 2.0–40.0 GeV/c.

Figure 3. Measured resolution on dE/dx for pion tracks from well reconstructed K^0_S decays. The points are for the real data and the histogram is for the Monte Carlo simulation normalised to the same number of tracks as the data.

Figure 4. Overall two-particle invariant mass spectra for (a) $K^{\pm}\pi^{\mp}$, (b) K^+K^-, (c) $K^{\pm}\pi^{\pm}$, (d) $K^{\pm}K^{\pm}$; background-subtracted mass spectra for (e) $K^{\pm}\pi^{\mp}$ and (f) K^+K^-. The points show the OPAL data while the solid histograms give absolute predictions of Jetset72. The dotted histograms in (b) and (d) are for Jetset72 with Bose-Einstein correlations using the parameters from [20].

Figure 5. Overall background-subtracted Monte Carlo mass spectra for (a) $K^{\pm}\pi^{\mp}$ and (b) $\pi^+\pi^-$ showing some of the components making up the spectra. In figure 5(b) the η and η' contributions, which are about equal, are added together.

Figure 6. Overall two-particle invariant mass spectra for (a) $\pi^+\pi^-$, (b) $\pi^{\pm}\pi^{\pm}$; (c,d,e) background-subtracted mass spectrum for $\pi^+\pi^-$. The points show the OPAL data while the solid histograms in (a,b,c) give absolute predictions of Jetset72. The histogram in (d) shows the result of including Bose-Einstein effects in Jetset with the default parameter values, while in (e) the OPAL parameter values (from [20]) have been used.

Figure 7. Mass spectra for K^+K^- in three bins of scaled momentum, x_p, showing as histograms the results of the fits described in the text: (a) $0.01 < x_p < 0.15$, (b) $0.15 < x_p < 0.3$, (c) $0.3 < x_p < 1$.

Figure 8. Mass spectra for $K^{\pm}\pi^{\mp}$ with, as histograms, the results of the weighted least squares fits described in the text: (a) $0.005 < x_p < 0.025$, (b) $0.025 < x_p < 0.1$, (c) $0.1 < x_p < 0.15$, (d) $0.15 < x_p < 0.3$, (e) $0.3 < x_p < 1$.

Figure 9. Differential cross sections for (a) $\phi(1020)$ and (b) $K^*(892)^0$ production; the solid curves indicate the predictions of Jetset 7.2 with default parameters, the dotted curves give the Herwig 5.0 predictions and the dashed curves show Jetset 7.2 tuned as described in section 8.

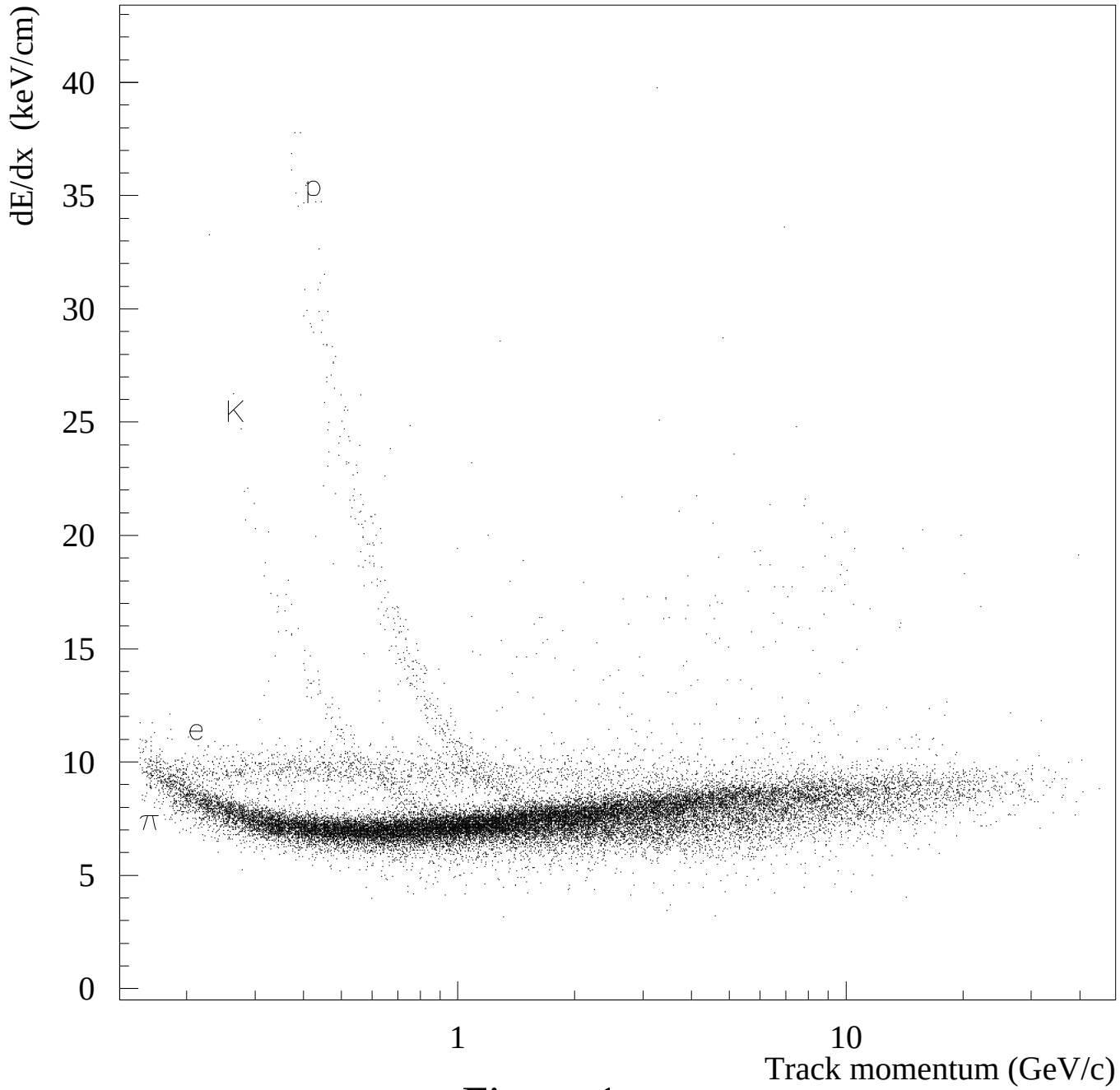

Figure 1

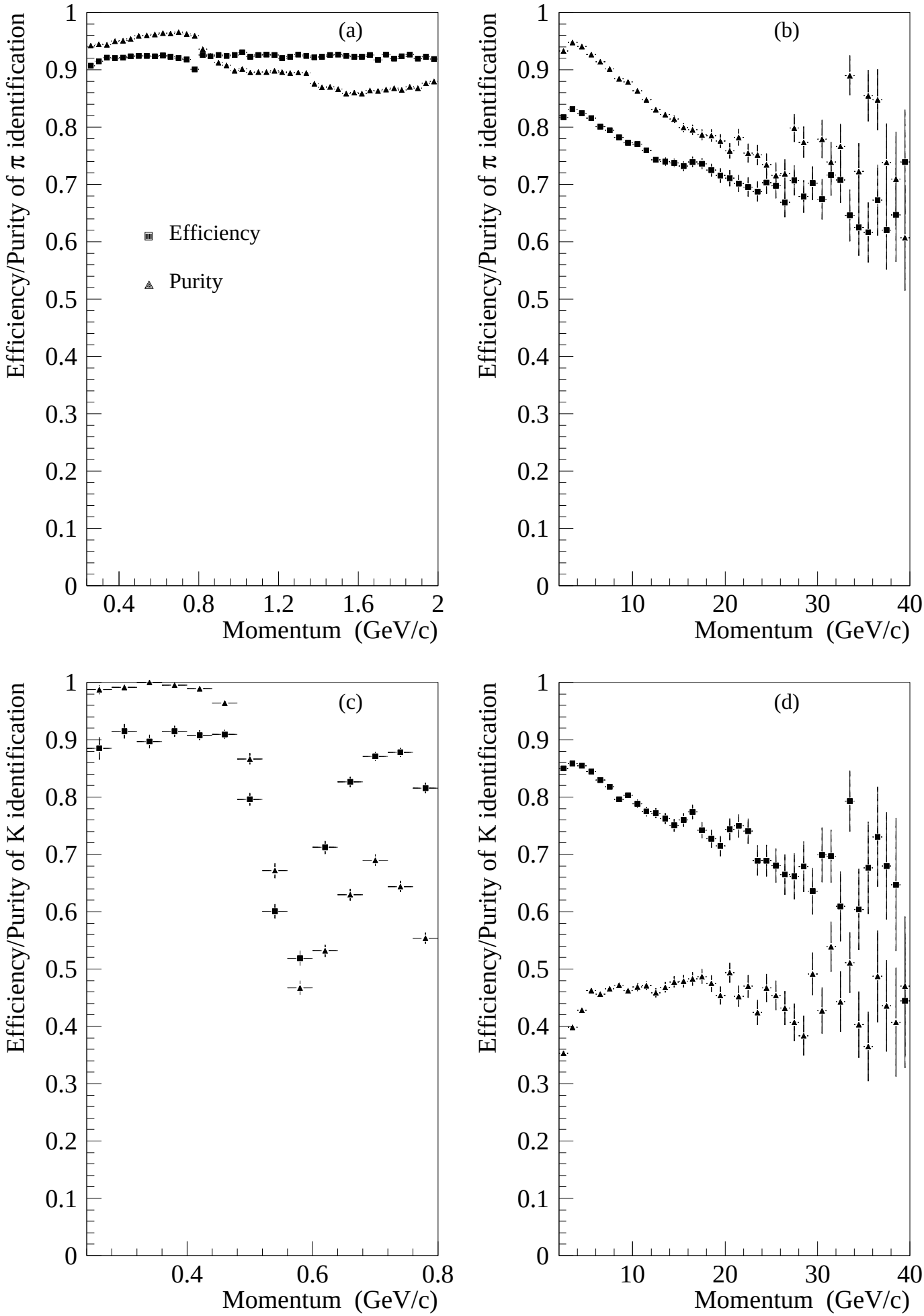
(a)
(b)
(c)
(d)
Efficiency
Purity
Efficiency/Purity of π identification
Efficiency/Purity of K identification
Momentum (GeV/c)

Figure 2

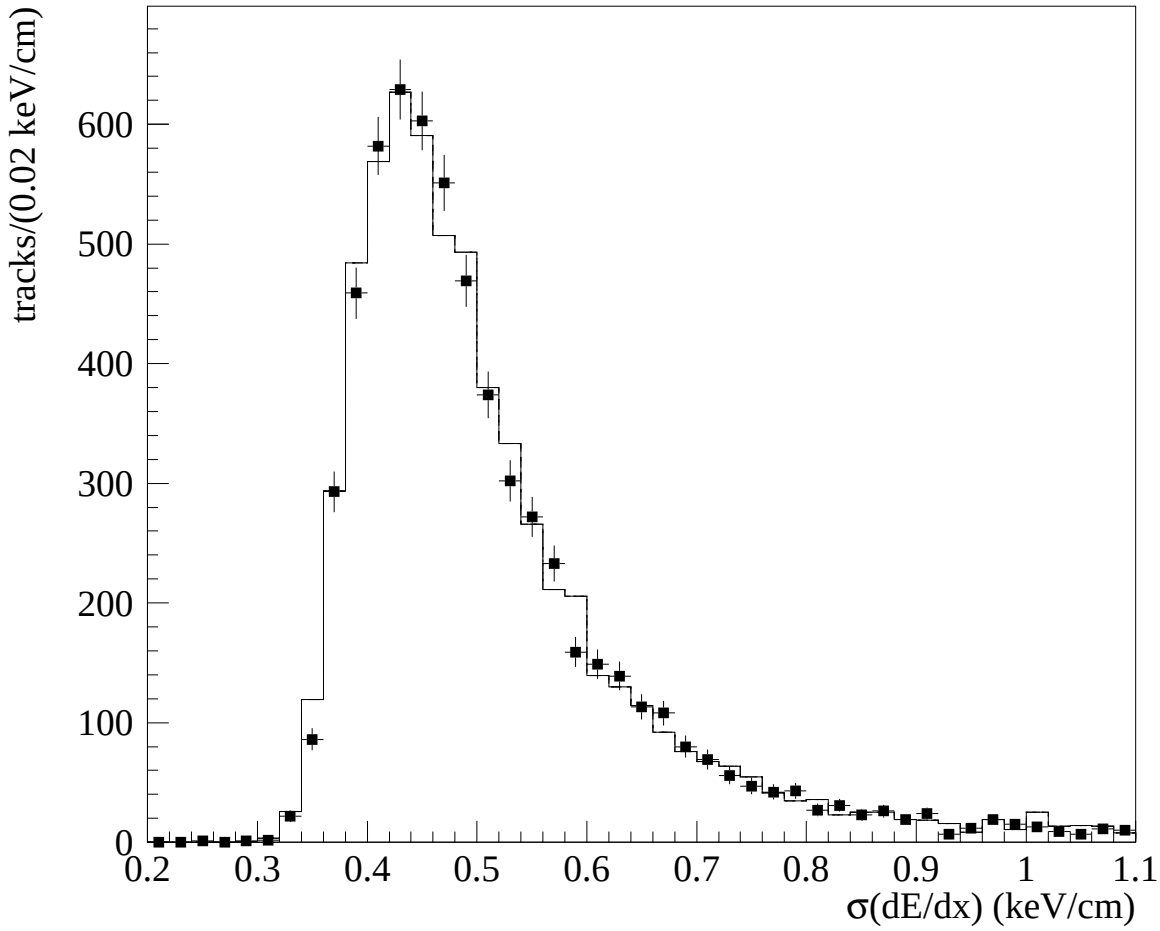
tracks/(0.02 keV/cm)
600
500
400
300
200
100
0
0.2
0.3
0.4
0.5
0.6
0.7
0.8
0.9
1
1.1
σ(dE/dx) (keV/cm)

Figure 3

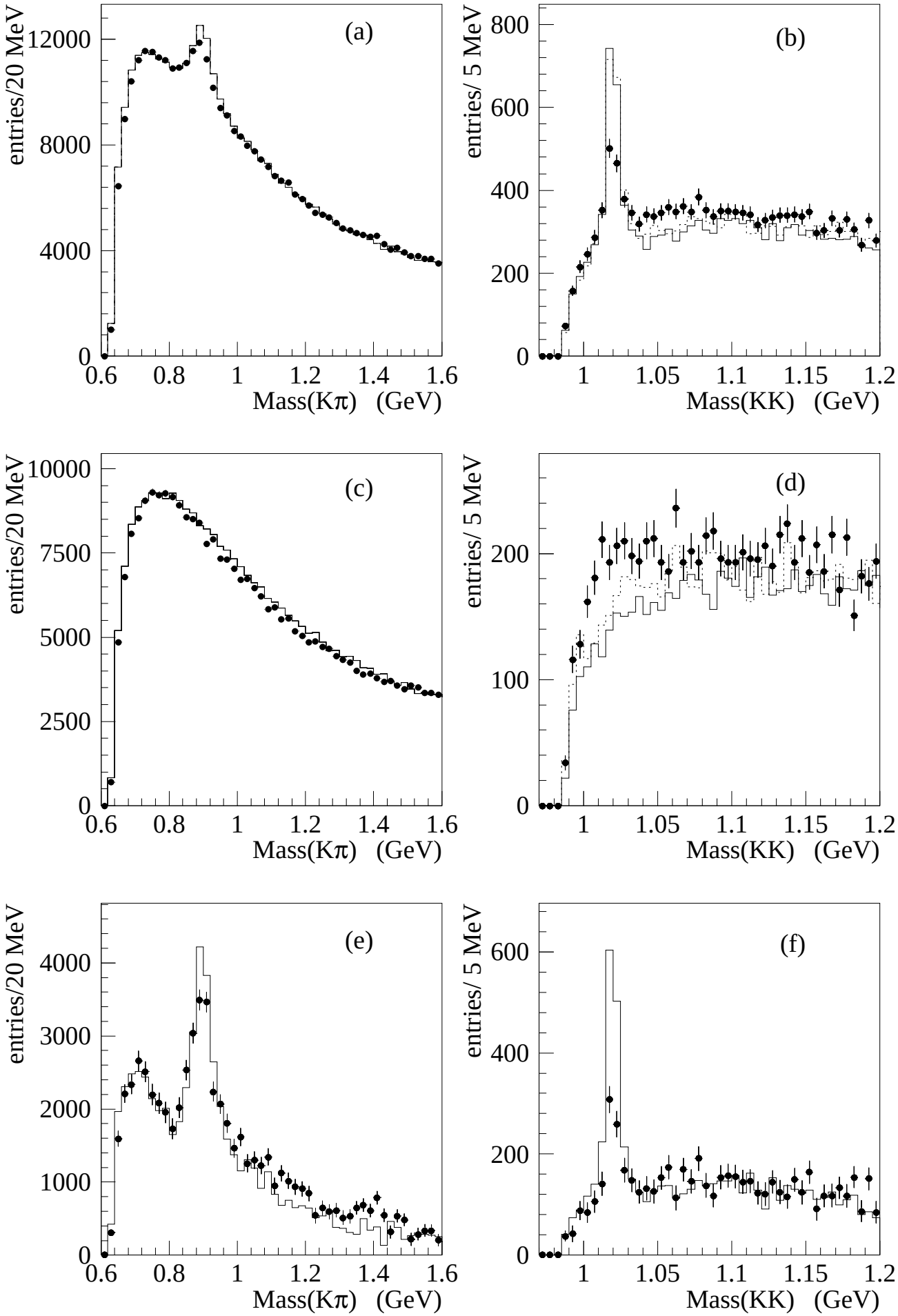
(a)
entries/20 MeV
Mass(Kπ) (GeV)
(b)
entries/ 5 MeV
Mass(KK) (GeV)
(c)
entries/20 MeV
Mass(Kπ) (GeV)
(d)
entries/ 5 MeV
Mass(KK) (GeV)
(e)
entries/20 MeV
Mass(Kπ) (GeV)
(f)
entries/ 5 MeV
Mass(KK) (GeV)

Figure 4

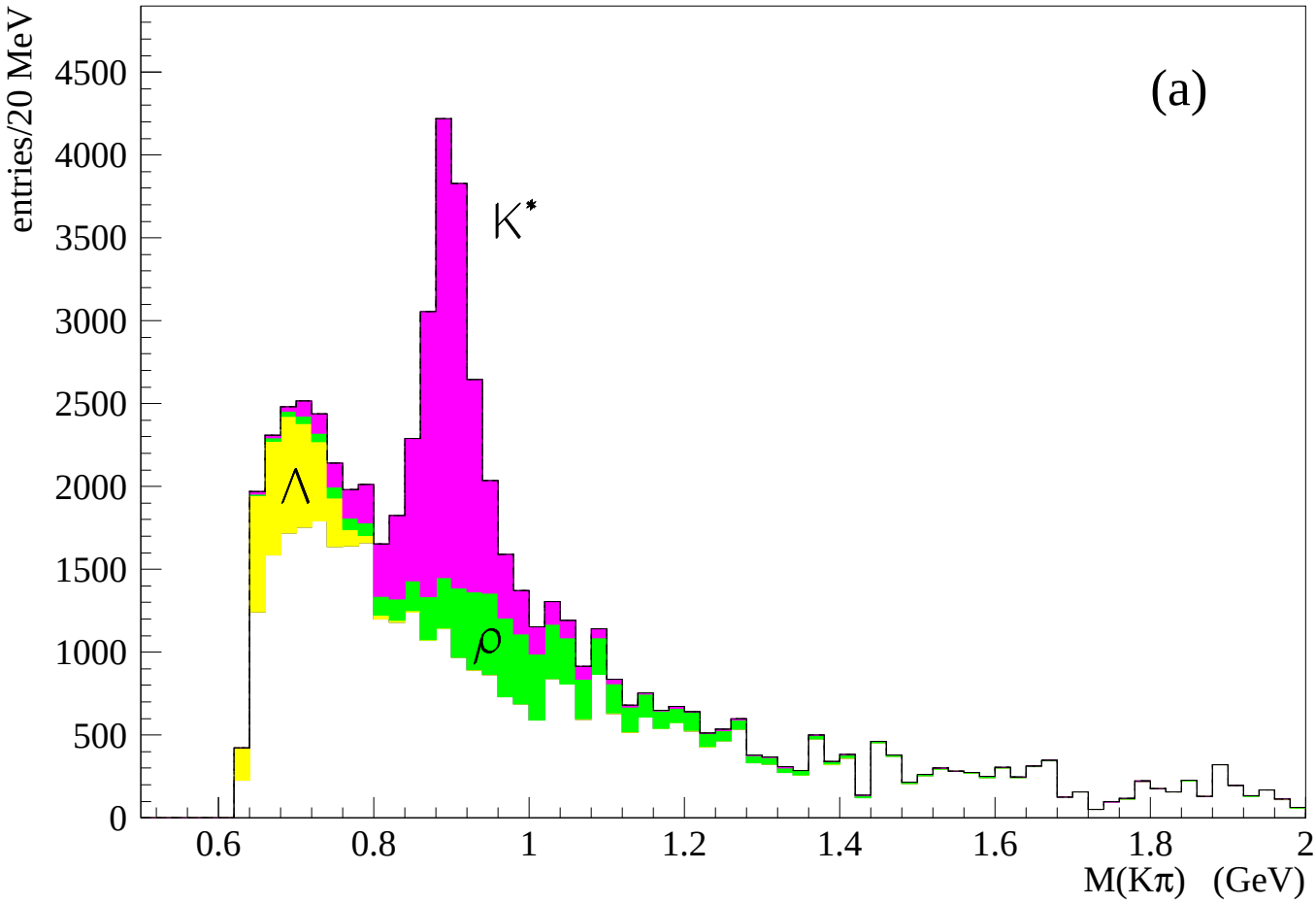
entries/20 MeV
4500
4000
3500
3000
2500
2000
1500
1000
500
0
0.6
0.8
1
1.2
1.4
1.6
1.8
2
M(Kπ) (GeV)
(a)
K*
Λ
ρ

Figure 5(a)

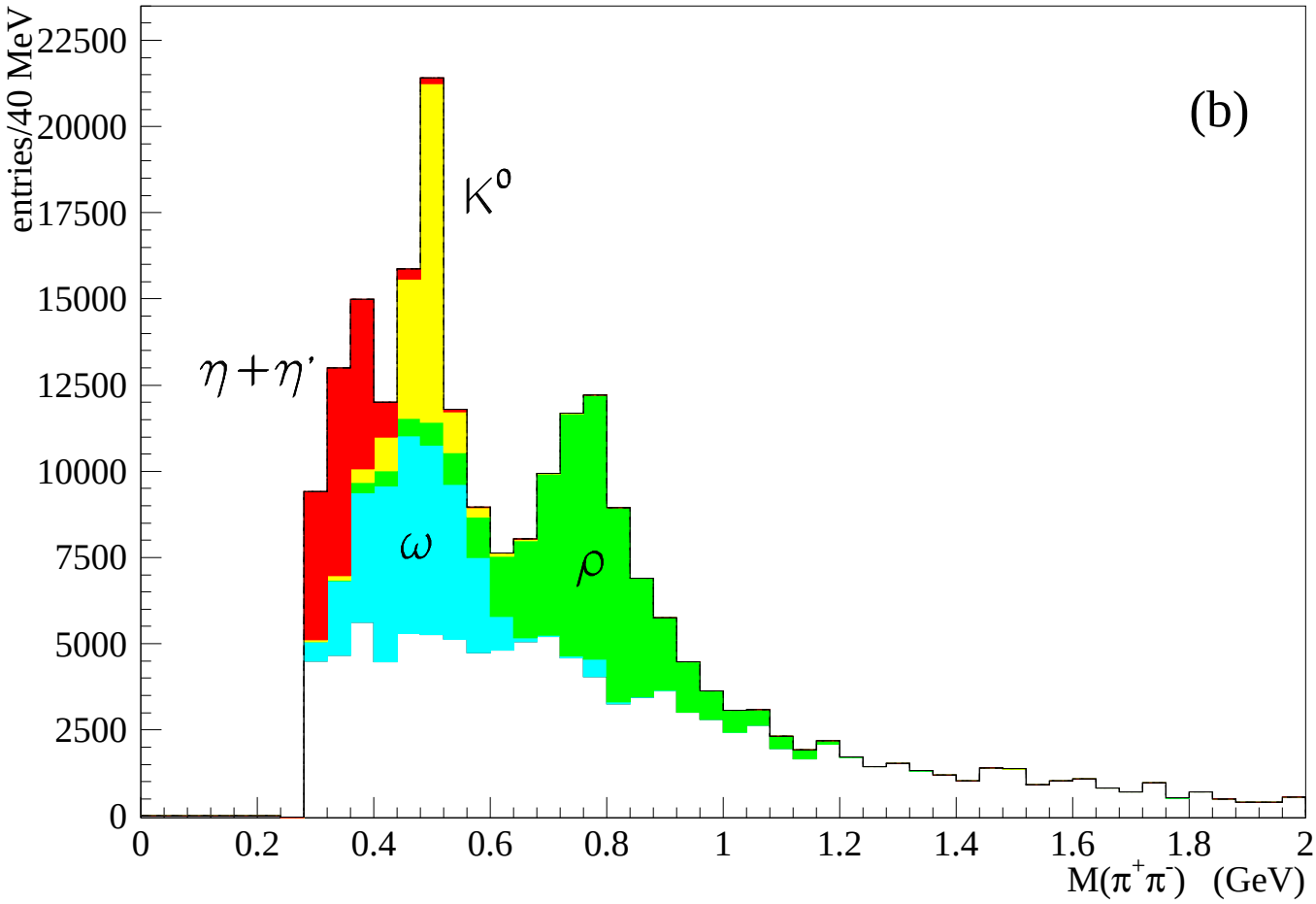
(b)
entries/40 MeV
22500
20000
17500
15000
12500
10000
7500
5000
2500
0
0
0.2
0.4
0.6
0.8
1
1.2
1.4
1.6
1.8
2
M(π+π-) (GeV)
η+η'
K0
ω
ρ

Figure 5(b)

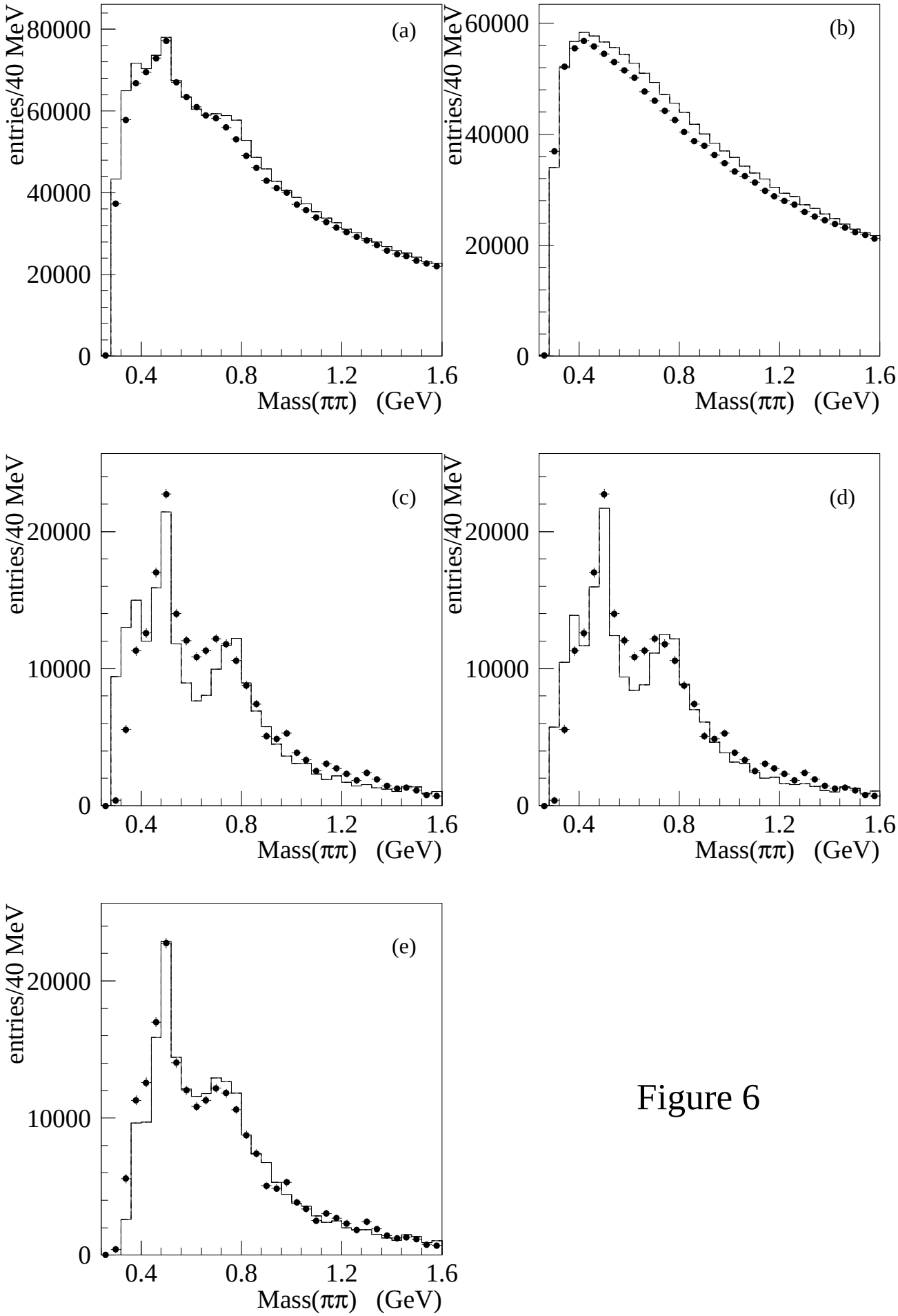
(a)
(b)
(c)
(d)
(e)
entries/40 MeV
Mass(ππ) (GeV)
0
20000
40000
60000
80000
10000
0.4
0.8
1.2
1.6

Figure 6

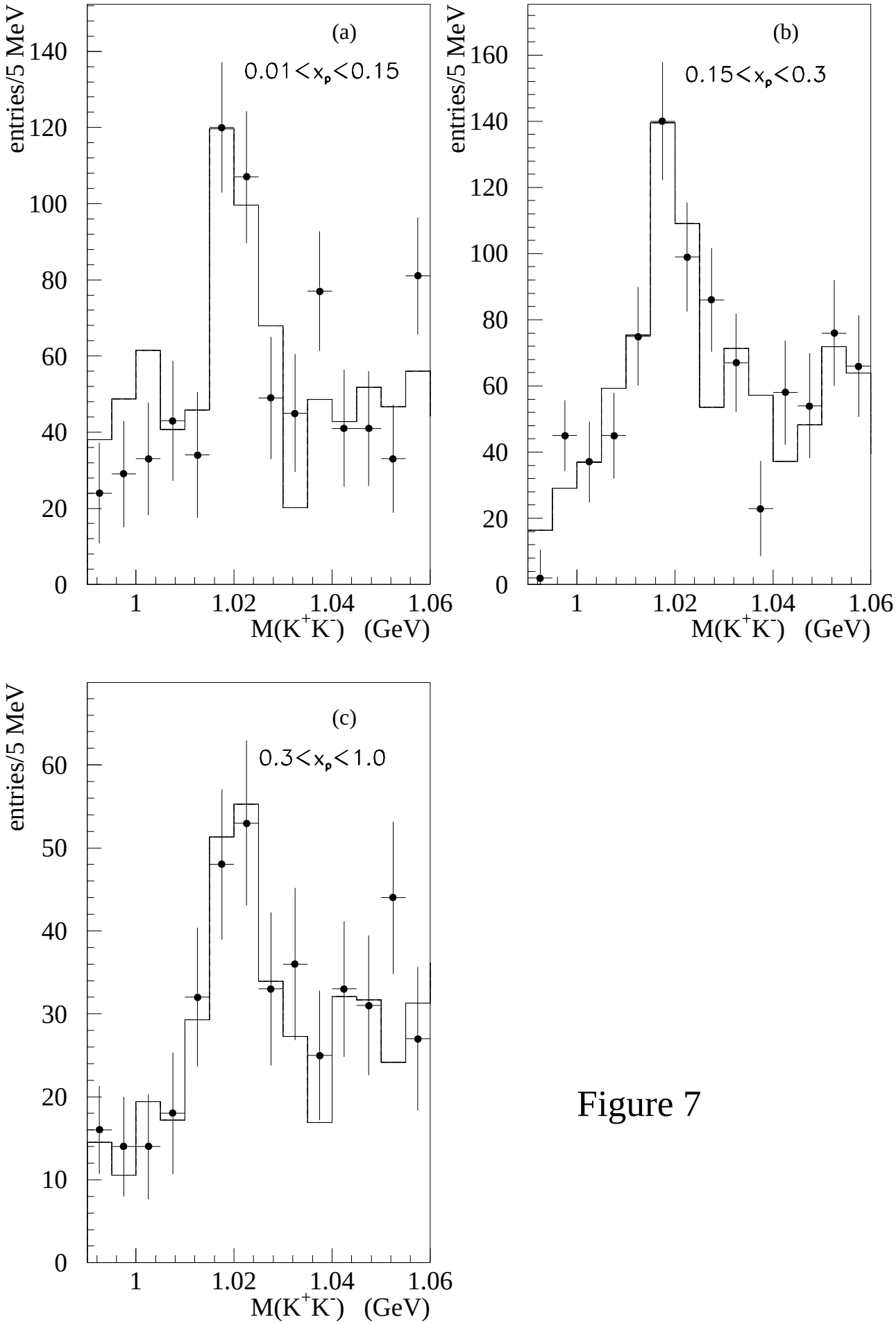
(a)
0.01<x_p<0.15
entries/5 MeV
M(K+K-) (GeV)
(b)
0.15<x_p<0.3
entries/5 MeV
M(K+K-) (GeV)
(c)
0.3<x_p<1.0
entries/5 MeV
M(K+K-) (GeV)

Figure 7

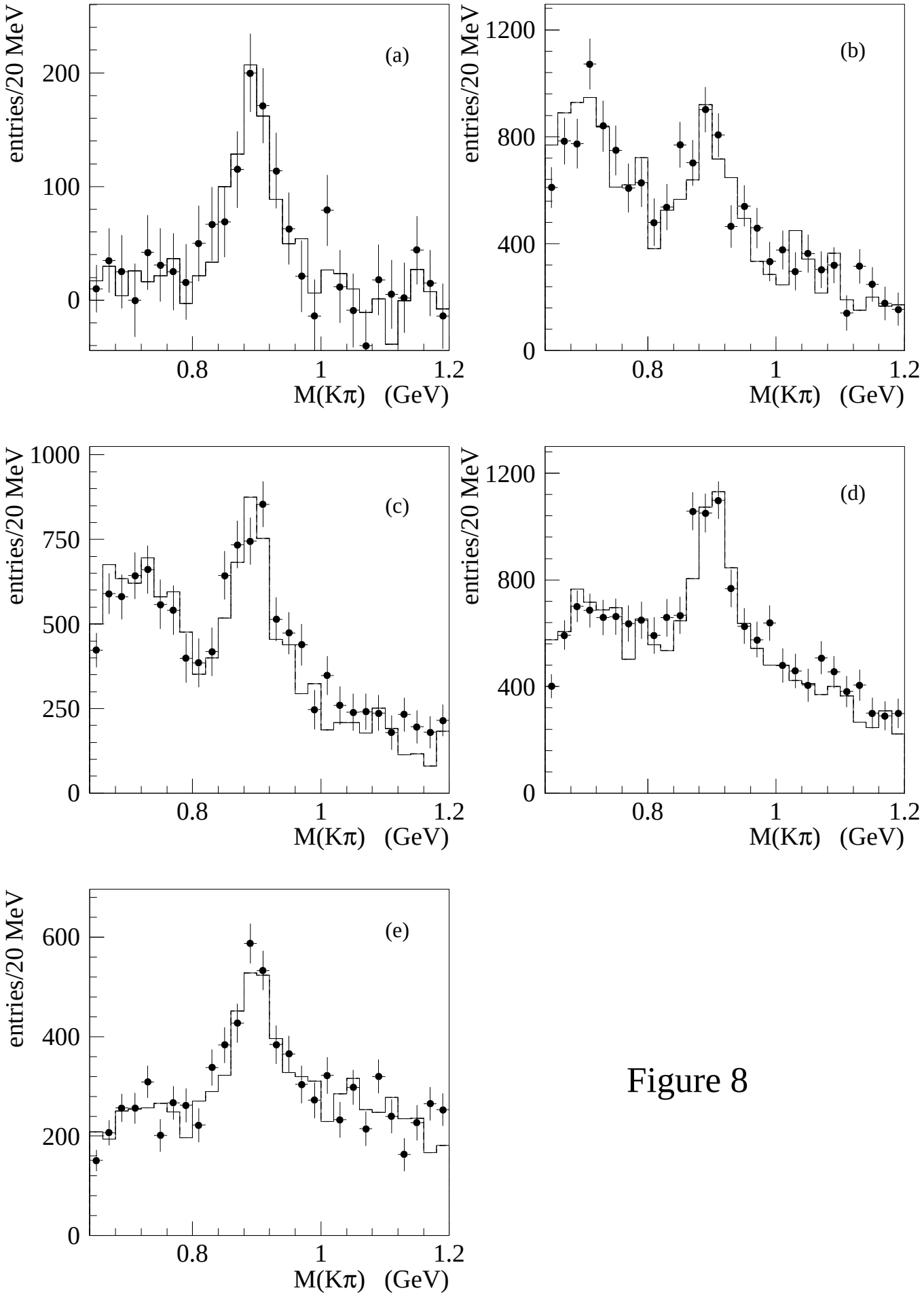

Figure 8

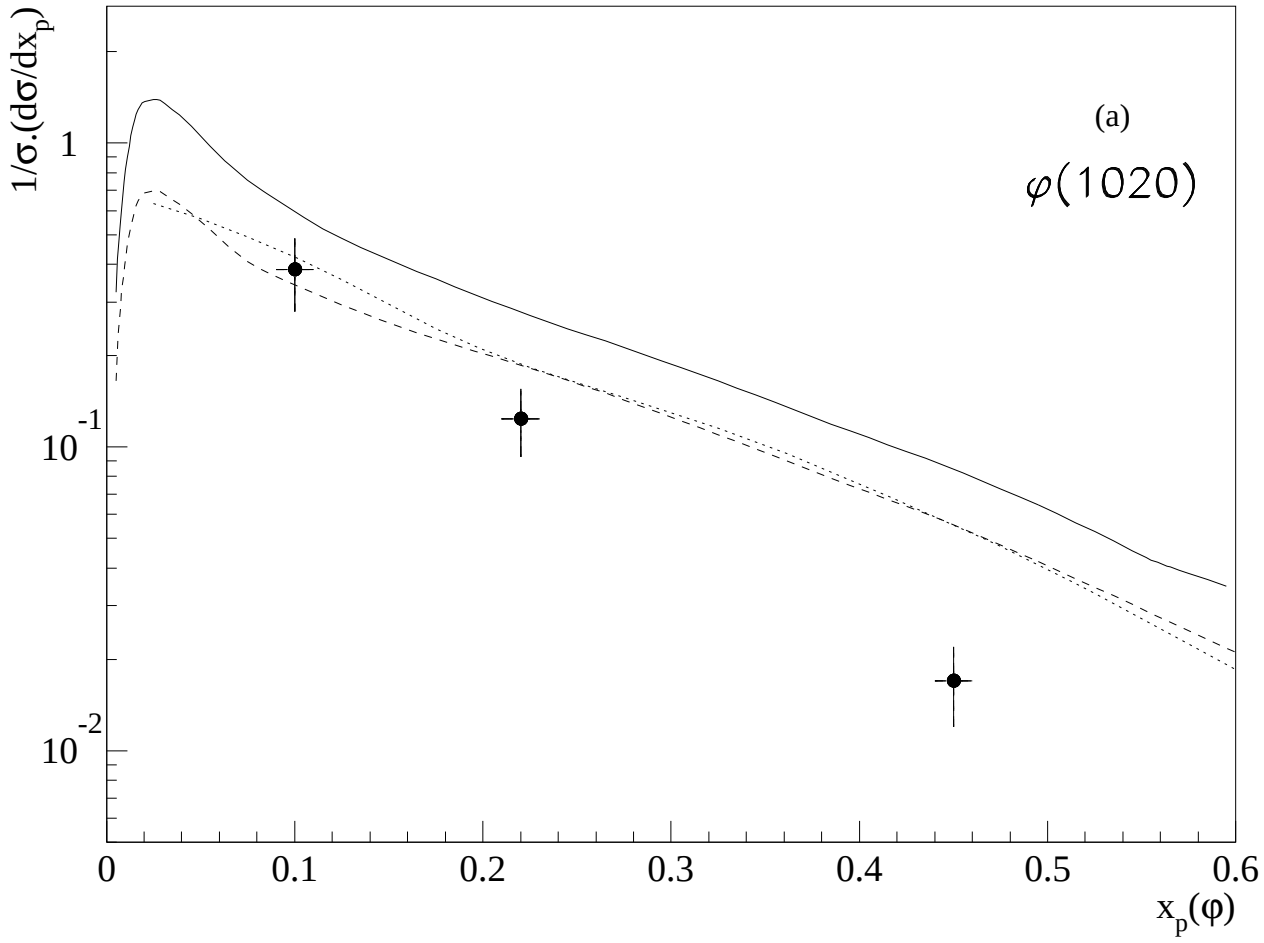
1/σ.(dσ/dx_p)
1
10^-1
10^-2
(a)
φ(1020)
0
0.1
0.2
0.3
0.4
0.5
0.6
x_p(φ)

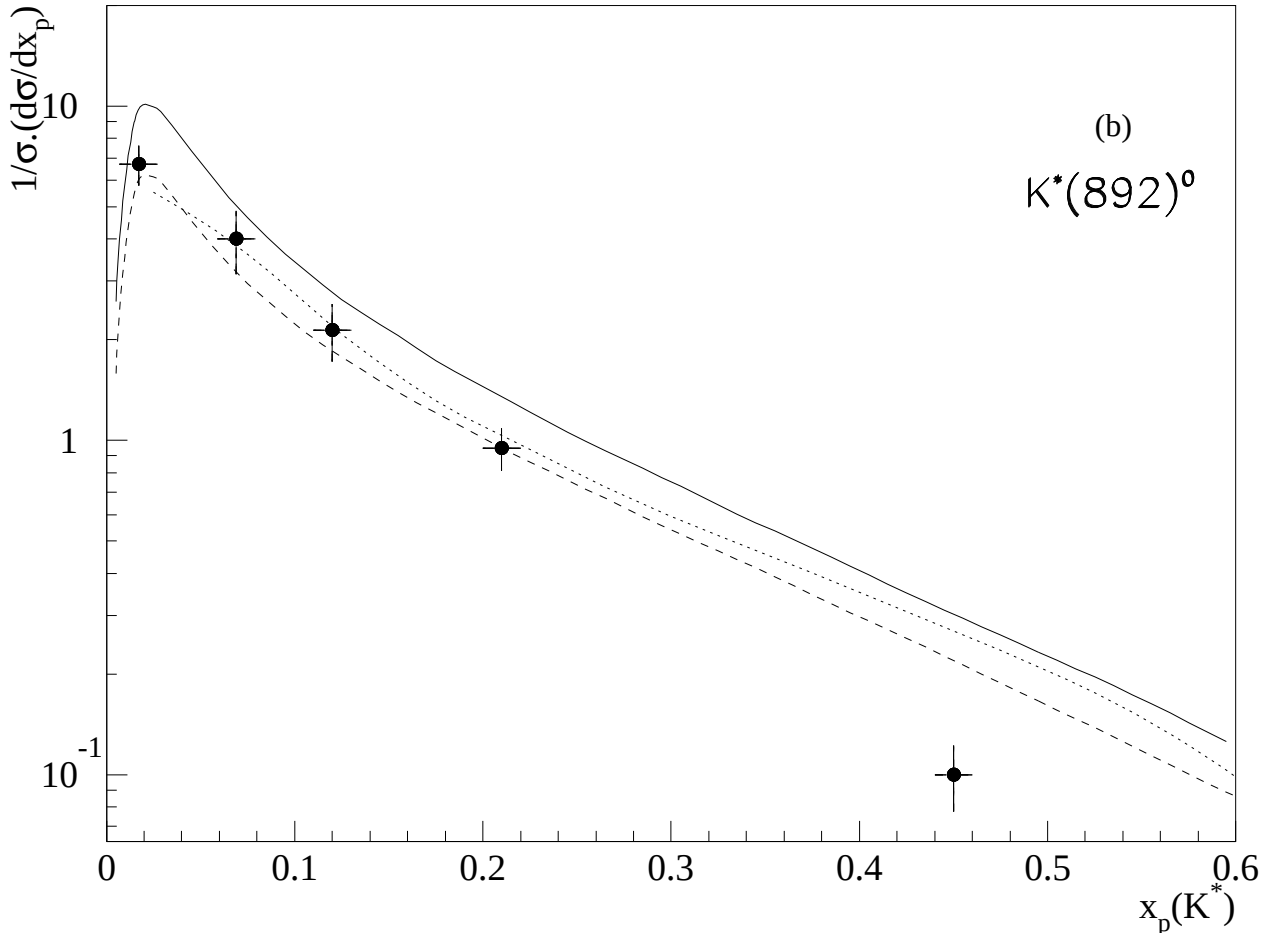
1/σ.(dσ/dx_p)
10
1
10^-1
(b)
K*(892)°
0
0.1
0.2
0.3
0.4
0.5
0.6
x_p(K*)

Figure 9